UNIVERSITY OF AMSTERDAM

UvA-DARE (Digital Academic Repository)

Solar-Driven Continuous CO_2 Reduction to CO and CH_4 using Heterogeneous Photothermal Catalysts

Recent Progress and Remaining Challenges

Schuurmans, Jasper .H.A.; Masson, T.M.; Zondag, S.D.A.; Buskens, P.; Noël, T.

DOI
10.1002/cssc.202301405

Publication date
2024

Document Version
Final published version

Published in
ChemSusChem

License
CC BY

Link to publication

Citation for published version (APA):
Schuurmans, J. . H. A., Masson, T. M., Zondag, S. D. A., Buskens, P., & Noël, T. (2024). Solar-Driven Continuous CO_2 Reduction to CO and CH_4 using Heterogeneous Photothermal Catalysts: Recent Progress and Remaining Challenges. *ChemSusChem*, *17*(4), Article e202301405. https://doi.org/10.1002/cssc.202301405

General rights
It is not permitted to download or to forward/distribute the text or part of it without the consent of the author(s) and/or copyright holder(s), other than for strictly personal, individual use, unless the work is under an open content license (like Creative Commons).

Disclaimer/Complaints regulations
If you believe that digital publication of certain material infringes any of your rights or (privacy) interests, please let the Library know, stating your reasons. In case of a legitimate complaint, the Library will make the material inaccessible and/or remove it from the website. Please Ask the Library: https://uba.uva.nl/en/contact, or a letter to: Library of the University of Amsterdam, Secretariat, Singel 425, 1012 WP Amsterdam, The Netherlands. You will be contacted as soon as possible.

UvA-DARE is a service provided by the library of the University of Amsterdam (https://dare.uva.nl)

Download date:27 May 2024

Check for updates

ChemSusChem

Review
doi.org/10.1002/cssc.202301405

Chemistry Europe
European Chemical Societies Publishing

www.chemsuschem.org

Solar-Driven Continuous CO_2 Reduction to CO and CH_4 using Heterogeneous Photothermal Catalysts: Recent Progress and Remaining Challenges

Jasper H. A. Schuurmans[+,a] Tom M. Masson[+,a] Stefan D. A. Zondag[+,a] Pascal Buskens,[b, c] and Timothy Noël*[a]

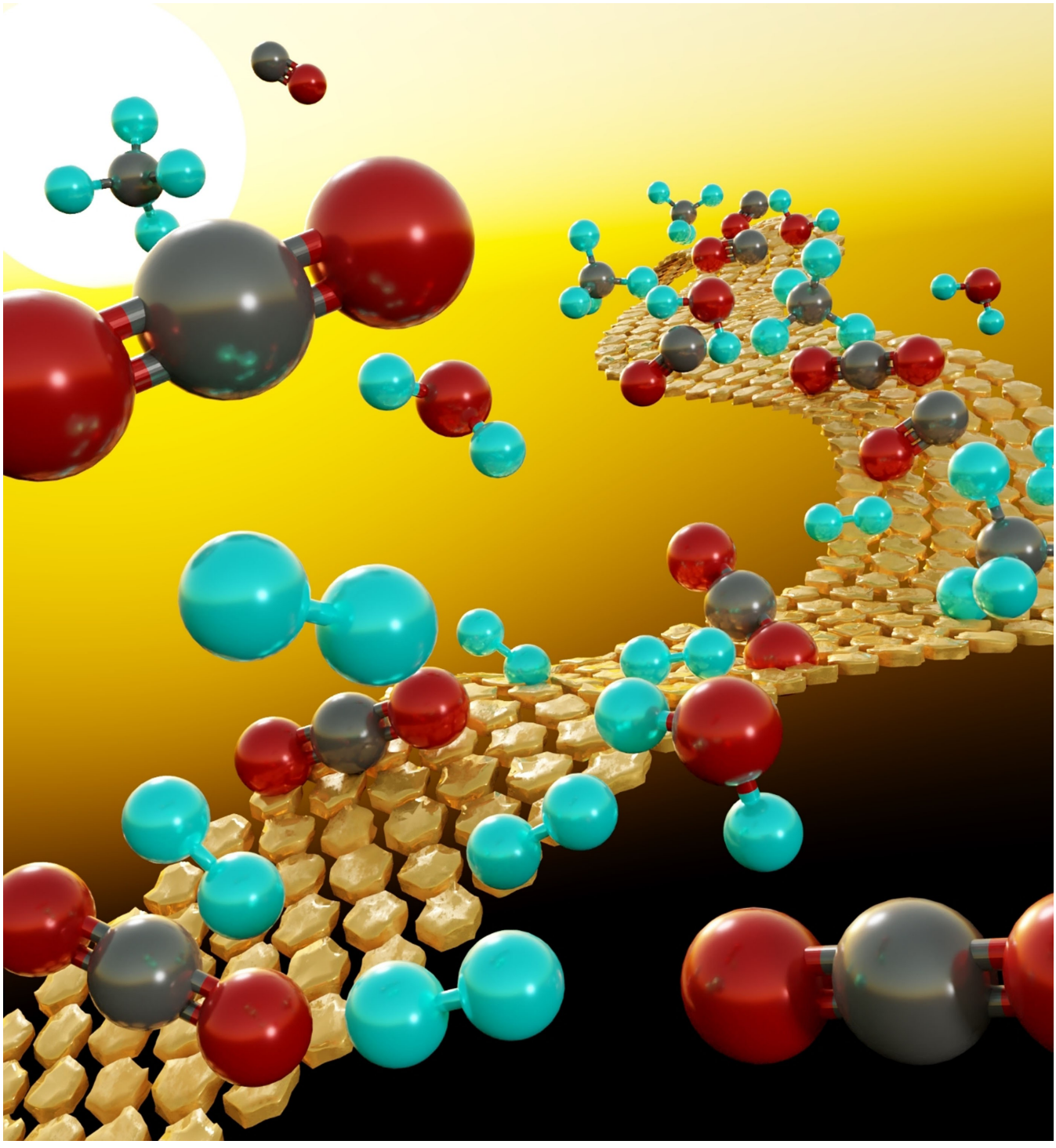

© 2023 The Authors. ChemSusChem published by Wiley-VCH GmbH

1864564x, 2024, 4, Downloaded from https://chemistry-europe.onlinelibrary.wiley.com/doi/10.1002/cssc.202301405 by Uva Universiteitsbibliotheek, Wiley Online Library on [02/05/2024]. See the Terms and Conditions (https://onlinelibrary.wiley.com/terms-and-conditions) on Wiley Online Library for rules of use; OA articles are governed by the applicable Creative Commons License

The urgent need to reduce the carbon dioxide level in the atmosphere and keep the effects of climate change manageable has brought the concept of carbon capture and utilization to the forefront of scientific research. Amongst the promising pathways for this conversion, sunlight-powered photothermal processes, synergistically using both thermal and non-thermal effects of light, have gained significant attention. Research in this field focuses both on the development of catalysts and continuous-flow photoreactors, which offer significant advantages over batch reactors, particularly for scale-up. Here, we focus on sunlight-driven photothermal conversion of CO_2 to chemical feedstock CO and CH_4 as synthetic fuel. This review provides an overview of the recent progress in the development of photothermal catalysts and continuous-flow photoreactors and outlines the remaining challenges in these areas. Furthermore, it provides insight in additional components required to complete photothermal reaction systems for continuous production (e.g., solar concentrators, sensors and artificial light sources). In addition, our review emphasizes the necessity of integrated collaboration between different research areas, like chemistry, material science, chemical engineering, and optics, to establish optimized systems and reach the full potential of this technology.

1. Introduction

The accumulation of greenhouse gases in the Earth's atmosphere is one of the most pressing environmental issues of our time.[1] In particular, the increase in atmospheric carbon dioxide (CO_2) concentrations has been linked to global warming and climate change.[2] According to the Intergovernmental Panel on Climate Change, the concentration of CO_2 in the atmosphere is currently at its highest level in at least 800,000 years (417.1 ppm in 2022), and the rate of increase has been accelerating over the past few decades. In the 1960s, the annual increase in atmospheric carbon dioxide concentration was about 0.8 ppm. The increase between 2021 and 2022 was 2.13 ppm, and it has been more than 2 ppm every year for the past decade. This trend is projected to have severe and potentially irreversible impact on the environment and human society, including rising sea levels, more frequent and severe weather events, and food and water scarcity.[3]

Mitigating the effects of climate change and limiting further damage requires a concerted effort around the world to transition to renewable energy sources, improve energy efficiency, and develop new technologies for carbon capture, storage, and conversion. Despite international efforts to reduce emissions and mitigate the effects of climate change, global CO_2 concentrations continue to rise due to increases in energy demand.[4] This makes it increasingly urgent to address this issue and actively work towards solutions that can remove excess CO_2 from the atmosphere.[5,6] In this context, chemists and chemical engineers have an important role to play in developing new synthetic methodologies that can capture and use CO_2 and convert it into added-value compounds. This not only helps to reduce CO_2 emissions but may also create new economic opportunities.[7–9]

However, it is important that these transformations are as efficient as possible, requiring a minimal energy input and producing minimal waste. To achieve this goal, researchers must adopt the principles of green chemistry and engineering,[10] which emphasize the design of chemical processes that are inherently safe, efficient, and sustainable.[11] Continuous-flow reactors have been evaluated to fulfill these requirements and contribute to more sustainable and greener processing, due to increased control and efficiency.[12,13]

In this review, we aim to provide an overview of recent research efforts to develop new chemical technologies to continuously convert CO_2 into useful CO and CH_4. We also highlight the direct use of sunlight as a clean and sustainable power source for these reactions. We review the performance of several semiconductors and metal nanoparticle based catalysts that have been developed and evaluated in recent years. Furthermore, we provide a detailed survey of continuous-flow reactors that have been proposed for these reactions, highlighting the various approaches to increase light collection, catalyst irradiation, and production. By presenting an overview of these technologies and their potential, we aim to contribute to a better understanding of the current state of the field and the challenges that need to be addressed to enable the widespread use of sunlight-driven CO_2 reduction.

2. CO_2 reduction pathways

Strategies aiming at converting carbon dioxide to useful chemicals and fuels are facing several obstacles, one being the stability of CO_2. Throughout the years, various processes were developed to address the challenge of CO_2 activation, for example, combining metal based catalysts with high temperatures. Two of the main reactions focused on in CO_2 reduction are the Sabatier reaction (Reaction 1) for methane (CH_4) production and the reverse water gas shift (RWGS) reaction

[a] J. H. A. Schuurmans,[+] T. M. Masson,[+] S. D. A. Zondag,[+] Prof. Dr. T. Noël
Flow Chemistry Group, Van't Hoff Institute for Molecular Sciences (HIMS)
University of Amsterdam
Science Park 904, 1098 XH Amsterdam, The Netherlands
E-mail: t.noel@uva.nl

[b] Prof. Dr. P. Buskens
The Netherlands Organization for Applied Scientific Research (TNO)
High Tech Campus 25, 5656 AE Eindhoven (The Netherlands)

[c] Prof. Dr. P. Buskens
Design and Synthesis of Inorganic Materials (DESINe), Institute for Materials Research
Hasselt University
Agoralaan Building D, 3590 Diepenbeek (Belgium)

[+] These authors contributed equally to this work.

© 2023 The Authors. ChemSusChem published by Wiley-VCH GmbH. This is an open access article under the terms of the Creative Commons Attribution License, which permits use, distribution and reproduction in any medium, provided the original work is properly cited.

(Reaction 2).[14–18] In the RWGS reaction carbon monoxide (CO) is produced, which can be used as feedstock for producing chemicals and fuels (e.g., methanol and Fischer-Tropsch hydrocarbons).[19–23] However, the use of high temperatures and pressures in combination with the use of non-sustainable energy in classical thermal processes encourages novel research to find alternative approaches.[24,25] Promising techniques as electrochemical reduction,[26–29] photoelectrochemical conversion[30,31] or photochemical transformation[15,32] are emerging as valuable potential alternatives to standard thermal approaches. The search for alternative techniques is also ongoing for other processes, such as dry reforming of methane.[33–35] This review will focus on the Sabatier and RWGS reaction, to show the application of green hydrogen, which has gained attention as one of the drivers for a carbon dioxide neutral energy economy.[36–38]

$$CO_2 + 4H_2 \rightarrow CH_4 + 2H_20 \quad (1)$$

$$CO_2 + H_2 \rightleftharpoons CO + H_2O \quad (2)$$

Natural photosynthesis uses solar light as energy source, inspiring academic research to use this form of renewable energy for chemical processes. The photons from sunlight can be used to drive the reduction of CO_2 in a continuous fashion, where reaction conditions are typically mild.[39] By using solar light, the energy consumption of the process can be directly lowered, and the short response times allow for on-demand

Jasper Schuurmans received his Bachelor of Science degree in Chemical Engineering and Chemistry and his Master of Science in Chemical Engineering (Chemical and Process Technology) at the Eindhoven University of Technology. His Master thesis was conducted in the Sustainable Process Engineering research group, focusing on multiphase photocatalytic reactions. At the moment, he is a Ph.D. candidate at the University of Amsterdam in the Flow Chemistry group, under the supervision of Prof. Timothy Noël, working on continuous-flow photoreactors.

Tom Masson received both his MSc and chemical engineering degrees from the Haute-Alsace University and the National Engineer school of Mulhouse. He worked on the synthesis of lipid kinase inhibitors as anticancer agents at the University of Basel. Later, he worked for Servier laboratories in Budapest on the synthesis of protein inhibitors as anticancer agents. For his MSc thesis Tom conducted work at Idorsia pharmaceuticals in Basel on the synthesis of new scaffolds to overcome immune suppression in cancer treatment. At Idorsia pharmaceuticals, he investigated the implementation of new methods of synthesis. Currently, he is a Ph.D. student at the University of Amsterdam working on heterogeneous photocatalysis in flow using concentrated light.

Stefan Zondag received both his Bachelor of Science degree in Chemical Engineering and Chemistry and his Master of Science degree in Chemical and Process Technology at Eindhoven University of Technology. During his Master he conducted research at Queen's University in Belfast, focused on hydrodynamic and acoustic cavitation technology. He finished his Master thesis on application and simulation of ultrasonic devices at the group of Micro Flow Chemistry & Synthetic Methodology in Eindhoven. Currently, he is a Ph.D. candidate at the University of Amsterdam, working on modelling of photochemical reactors.

Pascal Buskens (1980) received his Ph.D. degree in chemistry from RWTH Aachen University in 2006. After a five year career in industrial research with DSM, he rejoined RWTH Aachen University in 2012, where he successfully completed his habilitation in 2016. Since 2017, he combines a position as principal scientist at The Netherlands Organisation for Applied Scientific Research (TNO) with a guest professorship at Hasselt University. His main research interests are sunlight-powered photo(electro)chemical water splitting and CO2 reduction, as well as nanocomposite coatings and polymer films for smart windows and photovoltaics. Prof. Buskens contributed to the successful commercialization of multiple innovative coating products, (co−)authored more than 40 research articles and is inventor on more than 15 patents.

Timothy Noël is a Full Professor and Chair of Flow Chemistry at the University of Amsterdam, where he focuses on the delicate synergy between synthetic organic chemistry and technology. He has received several awards for his research in flow chemistry, including the DECHEMA prize (2017), the Hoogewerff Jongerenprijs (2019), the IUPAC-ThalesNano prize (2020), the KNCV Gold Medal (2021), the ACS Sustainable Chemistry & Engineering Lectureship Award (2022), and the ChemSocRev Pioneering Investigator Lectureship (2023). In addition, he serves as president of the Flow Chemistry Society and is co-organizer of #RSCPoster.

© 2023 The Authors. ChemSusChem published by Wiley-VCH GmbH

1864564x, 2024, 4, Downloaded from https://chemistry-europe.onlinelibrary.wiley.com/doi/10.1002/cssc.202301405 by Uva Universiteitsbibliotheek, Wiley Online Library on [02/05/2024]. See the Terms and Conditions (https://onlinelibrary.wiley.com/terms-and-conditions) on Wiley Online Library for rules of use; OA articles are governed by the applicable Creative Commons License

production.[40] Light can be absorbed by a photocatalyst, leading to several local events. For example, in a semiconductor material, an electron-hole pair can be formed if the energy of the light is higher than the material's band gap,[41] as illustrated in Figure 1. Generally, the UV region of the spectrum is energetic enough to excite stable metal oxide photocatalyst,[42] which can then participate in redox reactions with carbon dioxide and other reactants. However, only a small portion of the energy in the solar spectrum is UV (about 4%).[43] To work efficiently under solar light, a broad absorption range of the photocatalyst is required. Factors such as the crystal structure and morphology of the photocatalyst can affect the efficiency of solar light utilization and the absorption range.[44–46]

Apart from the highly-energetic UV region, also the visible and IR regions of the solar spectrum can serve different roles in the solar-driven conversion of CO_2. The visible part of the spectrum can contribute to the light absorption of the photocatalyst and promote charge separation,[47] while a broad range of the solar spectrum, including the IR region, can generate heat.[48–50] The resulting increased local temperature can be used as a driving force for a variety of reactions. To enhance this effect, metallic nanostructures can be added to, for example, contribute through direct intraband and interband electronic excitations.[48,51]

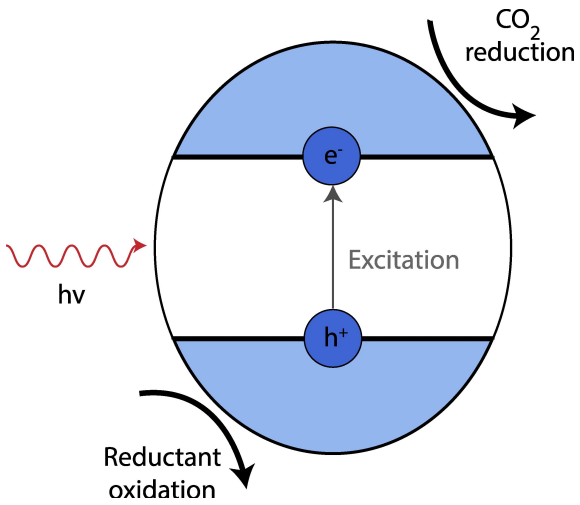

Figure 1. Representation of charge carrier formation and reaction over a semiconductor photocatalyst.

Using plasmonic metal nanoparticles on a semiconductor can increase activity through localized surface plasmon resonance (LSPR) excitation. Plasmonic nanoparticles have been shown to be good heating nanosources, when irradiated at their plasmonic resonance wavelength, which depends on the metal, size and shape of the nanostructure.[52,53] When irradiated, LSPR excitation generates strong localized electromagnetic fields that can enhance light absorption.[54,55] Decay of the LSPR can generate hot charge carriers that can be transported to the semiconductor, transferred to the adsorbate or convert their energy into heat.[48,56,57] Non-plasmonic metal nanoparticles can generate heat through similar pathways. In some cases, the hot carriers can react with substrates on the nanoparticle.[58] These processes and their timescales are illustrated in Figure 2, further details on the principles of plasmonic photothermal catalysis can be found in literature.[48,57,59–62] Overall, both the semiconductor and (plasmonic or non-plasmonic) metal nanoparticles can, upon illumination, contribute to the formation of heat or charge carriers, and external heating can also increase the apparent reaction rate.

The rate of a reaction can be increased through the photochemical contribution (reaction of reagents with formed charge carriers), which overcomes energy barriers.[63] However, supplying thermal energy can also improve the reaction rate by enhancing the mass transfer of the gas to the catalyst and making it easier for reactant molecules to overcome the activation barrier.[51] Therefore, the photothermal method, combining photochemical and thermal contributions, is often more efficient than a photochemical approach alone.

Properly ascribing irradiation effects and comparing thermal, photothermal, and photochemical situations can be challenging.[64–66] The heat generated by the catalyst can be spread across the entire sample, leading to a temperature increase, without any nanoscale features.[65,67,68] The rate of heat transfer to the environment and overall temperature profile is dictated by the thermal properties of the catalyst and the surroundings.[69–71] The latter includes the gas composition

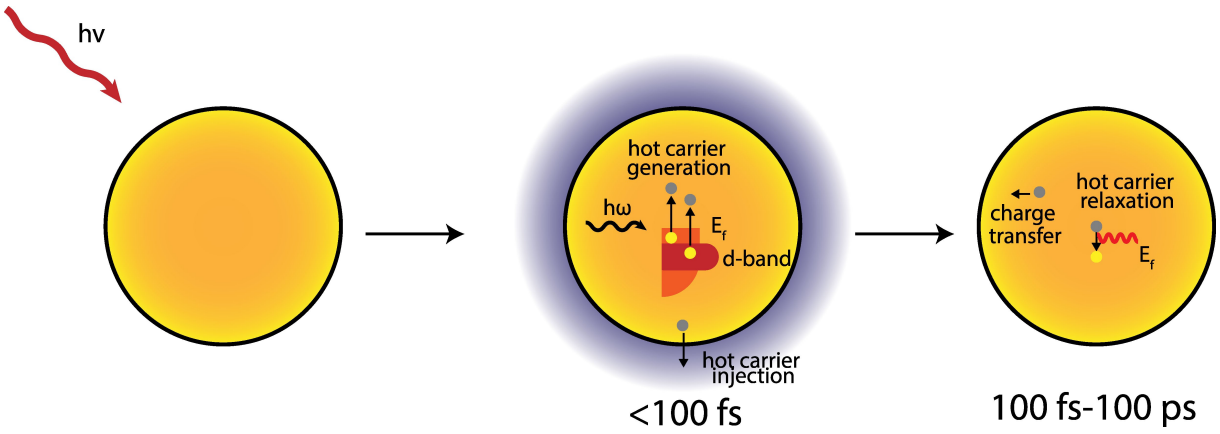

Figure 2. Processes of plasmonic nanoparticles on a semiconductor support and their timescales.

© 2023 The Authors. ChemSusChem published by Wiley-VCH GmbH

1864564x, 2024, 4, Downloaded from https://chemistry-europe.onlinelibrary.wiley.com/doi/10.1002/cssc.202301405 by Uva Universiteitsbibliotheek, Wiley Online Library on [02/05/2024]. See the Terms and Conditions (https://onlinelibrary.wiley.com/terms-and-conditions) on Wiley Online Library for rules of use; OA articles are governed by the applicable Creative Commons License

1864564x, 2024, 4, Downloaded from https://chemistry-europe.onlinelibrary.wiley.com/doi/10.1002/cssc.202301405 by Uva Universiteitsbibliotheek, Wiley Online Library on [02/05/2024]. See the Terms and Conditions (https://onlinelibrary.wiley.com/terms-and-conditions) on Wiley Online Library for rules of use; OA articles are governed by the applicable Creative Commons License

inside the reactor, as the different species in the CO_2 reduction reactions differ in thermal conductivity. For fundamental understanding of the process, it is important to account for the effect of localized heating on the catalyst bed to distinguish between thermal and non-thermal contributions of light. However, using a thermocouple may result in significant deviations from the actual local temperature, depending on the experimental conditions.[64,72,73] Therefore, reported temperatures may not always be reliable, and the overall evaluation of the catalyst should consider all experimental conditions, especially when willing to differentiate between the thermal and non-thermal contributions of the incident light.

To perform photothermal CO_2 conversion, several approaches can be taken. Water vapor can be used in the process, which is beneficial in terms of its abundance and non-polluting nature.[15] The use of water can be enabled through *in situ* photocatalytic water splitting into hydrogen, which then reduces the CO_2.[74] However, this approach has faced challenges due to undesirable reaction pathways, absorption mismatch between the catalyst and solar spectrum, and poor charge carrier separation and lifetimes, resulting in low CO_2 conversions.[75,76] To overcome these limitations novel reactor and catalyst development are key. This can include extending absorption bands, prolonging charge carrier lifetimes, exploring photothermal applications, and optimizing reactor design.[25,77,78] Instead of using water, green hydrogen can be used directly as a reductant to increase the efficiency and selectivity of the process.[49] Renewable hydrogen can be produced from water *ex situ* via other techniques, like (photo−)electrochemical water splitting,[79–81] making indirect use of the water.

The combination of carbon dioxide and the reductant allow for the formation of the desired products in the Sabatier and RWGS reaction. The choice of catalyst and operation conditions are crucial factors in the determination of the final efficiency and product distribution, where generally high selectivity is desired.[82] Hereby we describe relevant approaches to design catalysts to perform photothermal CO_2 reduction and we give an overview of the advancements in the field of reactor engineering necessary to meet posed challenges. The focus of this work will go out to catalysts that have been tested in continuous-flow, as these reactor types allow for better process control, higher inherent safety and more straightforward process intensification.[83–85] Overall, these reactors are more suitable for industrial applications and allow for a more straightforward and swift evaluation of the catalyst, in comparison to batch reactors.[86]

3. Catalysts for solar-driven CO_2 reduction

Common CO_2 reduction catalysts consist of a semiconductor or a support with a nanostructured metal. These catalysts can be synthesized through various procedures, such as wet impregnation, deposition-precipitation, chemical vapor deposition, and sol-gel methods.[87–90] The physical and chemical properties of the active sites of the catalyst have a significant impact on the activity and selectivity in CO_2 conversion by modulating the adsorption and desorption behavior of reactants, intermediates, and products.[33] The absorption range of the catalyst dictates, as mentioned, partially the efficiency of solar energy usage. Several classes of materials have been investigated in literature, some combining *in situ* water splitting with CO_2 conversion, others focusing solely on the conversion of carbon dioxide with hydrogen, the use of different feeds is illustrated in Tables 1–3, which gives an overview of photothermal catalysts that have been evaluated under (artificial) solar irradiation in continuous-flow systems.

3.1. Semiconductors

Metal oxides have been largely studied in literature due to their wide reactivity and large availability. Titanium dioxide (TiO_2) is frequently used because of its high activity and its ability to directly use water in the conversion of carbon dioxide. Even though TiO_2 typically absorbs low wavelengths (band gap of 3.2 eV for anatase TiO_2[91]), it has still been investigated as a solar photocatalyst as modifications of the material can increase the absorption at higher wavelengths.[92,93] Additionally, the UV part in the solar spectrum can be absorbed and used to form charge carriers. Nonetheless, the efficiency of solar energy usage is low when only the UV part or low wavelengths of the visible light part of the spectrum can be used, which might require more catalyst to obtain the desired productivity. The latter can be challenging in the scale-up of systems, posing technical and economic difficulties.[94,95]

The activity of different forms of TiO_2 has been investigated by Li and co-workers.[96] Upon irradiation, the catalyst dispersed on glass-fiber filters could convert the feed of carbon dioxide and water vapor to carbon monoxide and methane. The authors investigated the activity of nanocrystal polymorphs of pure TiO_2, including anatase, rutile, and brookite, for both defect-free and defective samples.[97] Rutile proved to be the least active, while the defective brookite polymorph resulted in the highest productivity, with selectivity towards CO. This result was attributed to the oxygen vacancies on the defective surface, which allowed for enhanced visible light absorption, as well as the presence of HCOOH intermediate on the brookite surface. Interestingly, this single-phase brookite TiO_2 has received limited attention in the literature, which prompted Li and co-workers to continue working on anatase and brookite polymorphs.[98] Both single-phase catalysts were investigated, as well as a mixed-phase anatase/brookite TiO_2 form and the commercially available anatase/rutile P25. In the comparison presented, the bicrystalline anatase/brookite outperformed both pure forms and P25, believed to be due to the interfaces between the anatase and brookite nanocrystals enhancing electron-hole separation and photo-induced charge transfer. This enhancement can also originate from the increased specific area of the composite bicrystalline TiO_2 compared to pure brookite.

In a subsequent study, the enhancement of electron-hole separation and available surface were further investigated for pure anatase TiO_2, with a primary focus on multi-facet TiO_2.[99]

© 2023 The Authors. ChemSusChem published by Wiley-VCH GmbH

Table 1. Overview of reported conditions and performance for continuous-flow solar-driven CO_2 reduction using water in literature.

Catalyst	Flow rate	Water content	Catalyst loading	Production	Temperature	Reactor	Light source	Ref
TiO_2 (defective brookite)	2 mL/min	~2.3 v%	100 mg	3.15 μmol/g_c/h ($CO + CH_4$)	–	Stainless-steel reactor with quartz window	150 W solar simulator ~90 mW/cm^2	[96]
TiO_2 (bicrystalline)	Not reported	~2.3 v%	100 mg	2.1 μmol/g_c/h (CO)	–	Stainless-steel reactor with quartz window	150 W solar simulator ~70 mW/cm^2	[98]
TiO_2 (defective multi-facet anatase)	4 mL/min	~2.3 v%	40 mg	UV-vis: 10.9 μmol/g_c/h (CO) vis: 5.3 μmol/g_c/h (CO)	150 °C	No details available Homemade reactor	UV-vis: 100 W Hg lamp vis: 450 W Xe lamp	[99]
Pt/TiO_2 (oxygen deficient P25)	40 mL/min (1 h) followed by 1 mL/min (5 h)	Described as moist CO_2	40 mg	80.35 μmol/g_c/h (CH_4)	Described as low-temperature	Stainless-steel reactor with quartz window	100 W solar simulation	[100]
Cu-Pt/TiO_2 (oxygen deficient P25)	40 mL/min (1 h) followed by 1 mL/min (5 h)	Described as moist CO_2	40 mg	500 μmol/g_c/h (CH_4)	–	Stainless-steel reactor with quartz window	100 W solar simulation	[119]
In_2S_3–TiO_2	20 sccm	Humidified	20 mg	435 μmol/g_c/h (CO) 94 μmol/g_c/h (CH_4)	150 °C	Spherical reactor	Concentrated sunlight	[201]
Cu_3–Fe/TiO_{23}–SiO_2	2.6 mL/min	CO_2 bubbled through distilled water	Thin layer coating	0.279 μmol/g_c/h (CH_4)	75 °C	Cylindrical Pyrex vessel with a quartz window and coated optical fibers.	Concentrated sunlight	[222]
N_{33}–Cu_3–Fe/TiO_2	2.6 mL/min	CO_2 bubbled through distilled water	Thin layer coating	0.617 μmol/g_c/h (CH_4)	75 °C	Cylindrical Pyrex vessel with a quartz window and coated optical fibers.	Concentrated sunlight	[223]
NiO/$InTaO_4$	5.8 mL/min (based on residence time and volume)	Saturated	125 mg	0.16 μmol/g_c/h (Methanol) 0.3 μmol/g_c/h (Acetaldehyde)	25 °C (Methanol) 70 °C (Acetaldehyde)	Internally illuminated optical fiber monolith reactor	300 W Xe lamp ~42 mW/cm^2	[224]
V/TiO_2	Not reported	Saturated	Thin layer coating	4.87 μmol/g_c/h (CH_4) 11.13 μmol/g_c/h (Acetaldehyde)	–	Internally illuminated optical fiber monolith reactor	500 W halogen lamp	[228]
Cu/TiO_2	1 L/min	25 mL/min	639 mg (1 wt% Cu)	> 2300 μmol/g_c/h (CO)	~800 °C	Tubular quartz monolith reactor	6.5 kW high-flux solar simulator ~153 suns	[225]
CdS–Cu^{2+}/TiO_2	4 mL/min	0.4 mL/min	Coating on TiO_2 nanorods	109.12 μmol/g_c/h (Ethanol)	80 °C	Optofluidic planar microreactor	300 W Xe lamp 40 mW/cm^2	[232]
Au_3–CN	3 mL/min	4.7 vol%	50 mg	6.6 μmol/g_c/h (CO) 1.6 μmol/g_c/h (CH_4)	–	Stainless steel photoreactor with quartz window	300 W Xe lamp	[128]
Cu_3–CNTs/pCN	5 mL/min	Saturated	150 mg	560 μmol/g_c/h (CO)	–	Continuous-flow fixed bed photoreactor	Solar simulator (100 mW/cm^2) with UV filters	[129]
Cu_3–$CsPbBr_3$	5.8 ml/min	Saturated	150 mg	14.7 μmol/g_c/h (CH_4)	300 °C	Custom-made photoreactor	300 W Xe lamp 300 mW/cm^2	[101]

© 2023 The Authors. ChemSusChem published by Wiley-VCH GmbH

1864564x, 2024, 4, Downloaded from https://chemistry-europe.onlinelibrary.wiley.com/doi/10.1002/cssc.202301405 by Uva Universiteitsbibliotheek, Wiley Online Library on [02/05/2024]. See the Terms and Conditions (https://onlinelibrary.wiley.com/terms-and-conditions) on Wiley Online Library for rules of use; OA articles are governed by the applicable Creative Commons License

Table 2. Overview of reported conditions and performance for continuous-flow solar-driven RWGS in literature.

Catalyst to CO	CO_2 flow	H_2 flow	Catalyst loading	Production	Temperature	Pressure	Reactor	Light source	Ref
$In_2O_{3-x}(OH)_y$	5 mL/min	5 mL/min	24 mg	15 μmol/g_c/h	150 °C	3 bar	Fixed-bed tubular reactor	300 W Xe lamp 2200 mW/cm^2	[107]
$In_2O_{3-x}(OH)_y$	5/15 mL/min	5/15 mL/min	20 mg	153 μmol/g_c/h	190 °C		Packed bed reactor	300 W Xe lamp 1000 W/m^2	[108]
$In_2O_{3-x}(OH)_y/SiO_2/Al$				14 μmol/g_c/h	160 °C		Annular reactor	3.5 kW Xe lamp 245.7 mW/cm^2	[175]
$In_2O_{3-x}(OH)_y/Ni$	15 sccm	15 sccm		755 μmol/g_c/h	295 °C		Foam structured reactor	3.5 kW solar simulator 1.8 suns	[231]
$In_2O_{3-x}(OH)_y$	1 sccm	5 sccm	Coated glass rod	246 μmol/g_c/h	200 °C	1 bar	Flow waveguide photoreactor	Xe arc lamp	[229]
Rhombohedral $In_2O_{3-x}(OH)_y$	2 mL/min	6 mL/min	20 mg	1.2 mmol/g_c/h	270 °C	1 bar	Tubular quartz reactor	130 W Xe lamp	[109]
Bi^{3+} *substituted* $In_2O_{3-x}(OH)_y$	1 sccm	1 sccm	20 mg	Approx. 100 μmol/g_c/h	190 °C		Fixed-bed tubular reactor	300 W Xe lamp	[110]
In_2O_{3-x}/In_2O_3	1 sccm	1 sccm	20 mg	161 μmol/m^2/h	300 °C	2.8 bar	Fixed-bed tubular reactor	300 W Xe lamp 8 suns	[111]
Pt nanoparticles on SiO_2	0.5 vol% 50 sccm CO2/N2	1.5 sccm	10 mg	5.4 mmol/g_{Pt}/h	300 °C	1 bar	Custom-made photoreactor	300 W Xe lamp 35 mW/cm^2	[40]
Rh nanoparticles on TiO_2	4 mL/min	16 mL/min	50 mg	21 mmol/g_c/h	250 °C	1 bar	Fixed-bed tubular reactor	300 W Xe lamp 2.7 W/cm^2	[135]
Au nanoparticles on TiO_2	67.5 mL/min	67.5 mL/min	75 mg	7423 mmol/m^2/h	200 °C	3.5 bar	Custom-made photoreactor	1440 mW/cm^2	[123]
Au nanoparticles on TiO_2	5 sccm	10 sccm	3–30 mg	2.7 mmol/g_{Au}/min (CO_2 conversion rate)	400 °C	7.6 bar	Harrick scientific (HVC-MRA-5)	Dolan-Jenner visible light source	[124]
$Pt_1Mo_{0.3}/SiO_2$	5 sccm	10 sccm	3–7 mg	1.6 mmol/g_c/min (CO_2 conversion rate)	200 °C	7.1 bar	Harrick scientific (HVC-MRA-5)	Dolan-Jenner visible light source	[150]
$AuMo/SiO_2$	5 sccm	10 sccm	3–5 mg	1.2 mmol/g_c/min (CO_2 conversion rate)	300 °C	8.1 bar	Harrick scientific (HVC-MRA-5)	Dolan-Jenner visible light source	[233]
$CuGa/CeO_2$	10 ml/min	10 ml/min	10 mg	111 mmol/g_c/h	280 °C		Flow-type reactor with external heating	1950 mW/cm^2	[234]
$Ni_{12}P_5/SiO_2$	2.5 sccm	0.5 sccm		13.3 mmol/g_c/h	290 °C		Tubular capillary reactor	300 W Xe lamp 0.8 W/cm^2	[151]
Cu_2O *nanocubes*	2.5 sccm	0.5 sccm		140 mmol/g_c/h		4 bar	LED flow reactor	LED, 50 suns (blue, green, and red)	[121]
Cu substituted HAP	1 sccm	1 sccm	10 mg	Approx. 750 μmol/g_c/h	300 °C	1 bar	Fixed-bed tubular reactor	300 W Xe lamp 2 W/cm^2	[122]
Pd/WO_3			9 mg	8.9 μmol/h	200 °C		Plug flow capillary reactor	120 W Xe lamp 2 W/cm^2	[130]

© 2023 The Authors. ChemSusChem published by Wiley-VCH GmbH

1864564x, 2024, 4, Downloaded from https://chemistry-europe.onlinelibrary.wiley.com/doi/10.1002/cssc.202301405 by Uva Universiteitsbibliotheek, Wiley Online Library on [02/05/2024]. See the Terms and Conditions (https://onlinelibrary.wiley.com/terms-and-conditions) on Wiley Online Library for rules of use; OA articles are governed by the applicable Creative Commons License

Table 2. continued

Catalyst to CO	CO_2 flow	H_2 flow	Catalyst loading	Production	Temperature	Pressure	Reactor	Light source	Ref
CuPd/WO$_3$	2 sccm	2 sccm		0.073 mmol/g$_c$/h	150 °C		Plug flow capillary reactor	120 W Xe lamp 2 W/cm^2	[132]
Encapsulated MOF-Fe nanoparticles	15 mL/min	15 mL/min		56 µmol/min	450 °C	1 bar	Fixed-bed reactor	Xe lamp	[153]
Pt/H$_x$MoWO$_y$	10 ml/min	10 ml/min	100 mg	3.1 mmol/g$_c$/h	140 °C		Fixed-bed reactor	300 W Xe lamp 0.88 W/cm^2	[131]

Treatment of the samples with $NaBH_4$ created oxygen vacancies, without significantly affecting the morphology and crystal facets. Co-exposed {101}-{001} facet surface heterojunctions with point defects enhanced charge separation and extended visible light absorption through additional intra-band gap energy states. This change in absorption capabilities was also apparent from the resulting blue color of the catalyst. Another blue-colored oxygen deficient TiO_2 was also obtained by In and co-workers, where commercial P25 TiO_2 was treated with varying amounts of $NaBH_4$ to obtain various degrees of reduced (blue) titania.[100]

Other semiconductors than TiO_2 can be investigated to obtain a more efficient use of the solar spectrum. This is the case for halide perovskites semiconductors that have emerged as promising catalysts for solar CO_2 reduction. The use of interstitial copper dopants in $CsPbBr_3$ was shown to increase the activity of the perovskite catalyst by suppressing recombination of charge carriers and promoting CO_2 adsorption and activation.[101] Similarly, graphitic carbon nitride (g-C_3N_4), a metal-free conjugated semiconductor,[102–104] can be used as catalyst, as it has a moderate band gap (2.7–2.8 eV[105]) in comparison to TiO_2, resulting in better visible light absorption.[106]

For the selective production of carbon monoxide, altered indium oxide (In_2O_3) can be used as catalyst in the RWGS reaction. The optoelectronic structure, including crystal phase, size, morphology, doping elements, and defect concentrations, have been investigated.[78] In one study, researchers discovered that the catalyst's activity is strongly associated with the surface populations of hydroxides and oxygen vacancies, which are essential for CO_2 adsorption and charge transfer.[107] The catalyst is often described as cubic $In_2O_{3-x}(OH)_y$, when it contains a high concentration of hydroxides and oxygen vacancies, earning the name defect-laden indium oxide. Experimental studies and density functional theory (DFT) simulations were performed to understand the mechanism of the RWGS reaction on this catalyst. The proposed mechanism (see Figure 3) suggests that the heterolytic splitting of hydrogen occurs on adjacent Lewis base hydroxide and Lewis acid indium sites, located near a surface oxygen vacancy.[108] Proton and hydride transfer to adsorbed carbon dioxide ultimately produces the RWGS reaction products.

Apart from the cubic, the rhombohedral form of indium oxide does also show high activity as photocatalyst in the RWGS reaction.[109] This catalyst does not only produce carbon monoxide but also methanol and has been shown to be stable over long periods of time. The improved catalytic performance is attributed to the increased acidity and basicity of surface frustrated Lewis pairs in the rhombohedral form compared to the cubic polymorph.

The photocatalytic activity of altered indium oxide hydroxide can be further increased through various methods. For instance, one study focused on the isomorphous substitution of In^{3+} with Bi^{3+}.[110] DFT analysis suggested that, at the optimal substitution level, the Lewis basicity of the basic site was mildly increased without affecting the acidity of the frustrated Lewis pair, maximizing the heterolytic splitting of

© 2023 The Authors. ChemSusChem published by Wiley-VCH GmbH

1864564x, 2024, 4, Downloaded from https://chemistry-europe.onlinelibrary.wiley.com/doi/10.1002/cssc.202301405 by Uva Universiteitsbibliotheek, Wiley Online Library on [02/05/2024]. See the Terms and Conditions (https://onlinelibrary.wiley.com/terms-and-conditions) on Wiley Online Library for rules of use; OA articles are governed by the applicable Creative Commons License

Table 3. Overview of reported conditions and performance for continuous-flow solar-driven CO_2 methanation in literature.

Catalyst to CH_4	CO_2 flow	H_2 flow	Amount of catalyst	Production Conversion	Temperature	Reactor	Light source	Ref
Ru nanoparticles on SiO_2	0.5 vol% 50 sccm CO2/N2	1.5 sccm	10 mg	36 mmol/g_{Ru}/h	300 °C	Custom-made photoreactor	300 W Xe 35 mW/cm^2	[40]
Ni on $TiO_{2-x}H_x$	1 (–)	4 (–)	40 mg	**90 %**	441 °C	Quartz photothermal reactor	300 W Xe	[117]
Ni/Al_2O_3	1.5 mL/min	6 mL/min	20 mg	279 mmol/g_c/h	290 °C	Stainless reaction chamber with quartz window	300 W Xe 2.6 W/cm^2	[144]
RuO_2 nanoparticles on $SrTiO_3$	5 mL/min	20 mL/min	150 mg	200 μmol/g_c/h	150 °C	Glass column heated with a jacket	300 W Xe 1.1 W/m^2	[137]
Ni nanoparticles on SiO_2–Al_2O_3	1 mL/min	4 mL/min	100 mg	35 mmol/g_{Ni}/h (65% Ni loading) **75 %**	225 °C	Fixed bed reactor quartz rectangular cell	Single wavelength LED, 7–2200 mW/m^2	[214]
Ru nanorods on Al_2O_3	2 mL/min	9 mL/min	200 mg	264 μmol/min 792 mmol/g_{Ru}/h **45 %**	218 °C	Fixed bed reactor	AM 1.5 14.4 suns	[136]
Ni–Al_2O_3/SiO_2	0.4 mL/min	2 mL/min	200 mg	5 μmol/min **3.5 %**	225 °C	Glass column with a jacket	300 W Xe lamp 2327 W/m^2	[213]
Ru layered double hydroxide	5 mL/min	20.5 mL/min	150 mg	2.7 mmol/g_c/h **82 %**	350 °C	Glass cell, fixed bed photoreactor	300 W Xe lamp 10 suns	[145]
Ru on MIL-125(Ti)–NH2	4 mL/min	16 mL/min	50 mg	21.6 mmol/g_c/h	200 °C	Glass column with a jacket	150 W Hg-Xe lamp filter cut-off $\lambda > 420$ nm 1340 mW/cm^2	[235]
Co on La_x–TiO_2	4 mL/min	16 mL/min	45 mg	7 mmol/g_c/h **35 %**	450 °C	Harrick reactor	LED 0.3–0.5 W/cm^2	[148]
Co and Cu on CeO_2	4 mL/min	16 mL/min	100 mg	14400 mL/g_c/h **60 %**	450 °C	Harrick reactor	Blue LED 0.5 W/cm^2	[147]
Ni/Y_2O_3	2.5 mL/min	10 mL/min	100 mg	7.5 L/m^2/h **80 %**	288 °C	Quartz tube reactor	Xe lamp 1 sun/ real sunlight	[230]
Ir nanoparticles immobilized in UiO-66 MOF	4 mL/min	16 mL/min	50 mg 1.2 g quartz sand	20 mmol/g_c/h **9.3 %**	250 °C	Packed bed in a quartz reactor	300 W Xe lamp 2.4 W/cm^2	[154]
Ni/TiO_2	4 mL/min	16 mL/min	100 mg	– **56 %**	400 °C	Catalyst layer deposed on aluminum plate	300 W Xe lamp	[146]
Pb nanocrystals on Nb_2O_5 nanorods	0.2–2 sccm	0.2–2 sccm	5.6 mg	CH_4: 0.11 mol/g_{Pd}/h CO: 0.75 mol/g_{Pd}/h	160 °C	Cylindrical glass reactor based on a CSTR	300 W Xe lamp 2.1 W/cm^2	[152]
Ru/Natural halloysite nanotubes	5 ml/min	20 ml/min	5 mg	1704 mmol/g_c/h	327 °C	Continuous-flow photoreactor	300 W Xe lamp 2.1 W/cm^2	[149]
Ru/H_xMoO_{3-y}	5 ml/min	5 ml/min	150 mg	20.8 mmol/g_c/h	140 °C	Flow reactor with quartz window	Xe lamp 0.75 W/cm^2	[50]
Ni/Nb_2C	2 ml/min	2 ml/min		0.15 mol/g_{Ni}/h (CO_2 conversion rate)		Flow reactor with quartz window	15 suns	[138]

© 2023 The Authors. ChemSusChem published by Wiley-VCH GmbH

1864564x, 2024, 4, Downloaded from https://chemistry-europe.onlinelibrary.wiley.com/doi/10.1002/cssc.202301405 by Uva Universiteitsbibliotheek, Wiley Online Library on [02/05/2024]. See the Terms and Conditions (https://onlinelibrary.wiley.com/terms-and-conditions) on Wiley Online Library for rules of use; OA articles are governed by the applicable Creative Commons License

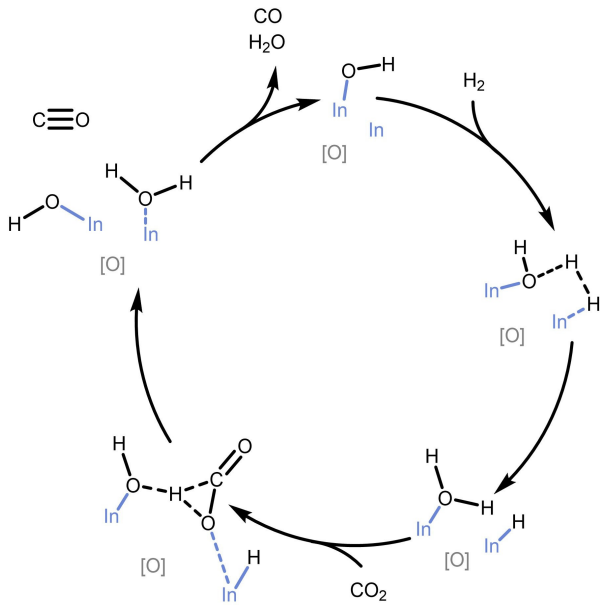

Figure 3. Overall proposed mechanism for the $CO_2 + H_2 \rightleftharpoons CO + H_2O$ reaction on $In_2O_{3-x}(OH)_y$. Adapted with permission from ref [108]. Copyright 2015 Royal Society of Chemistry.

hydrogen. Another approach investigated the effect of the color of defect-laden indium oxide to take advantage of the full spectrum of solar irradiation.[111] Researchers found that converting In_2O_3 into an oxygen-deficient, non-stoichiometric form (i.e., In_2O_{3-x}/In_2O_3) significantly darkened its color, resulting in stronger solar energy harvesting ability and photothermal effects.

3.2. Supported metal nanostructures

As mentioned before, the introduction of (plasmonic) metal nanostructures can increase the performance of the catalyst through thermal and non-thermal contributions.[112–114] The catalyst support material and characteristics are an important factor in these contributions, as the support can accept hot carriers formed on the metal nanostructures, which are transferred over the potential energy barrier between the metal and semiconductor, also referred to as the Schottky junction.[48] This can slow down the recombination of the charge carriers formed.[115] The metal nanostructures can also act as electron sinks by accepting electrons from the support, exemplifying the numerous interactions between the metal and the support.[42,116] Additionally, the adsorption of CO_2 at the surface of the catalyst is affected by the support material, where, for example, oxygen vacancies can play an important role in the adsorption and activation of CO_2.[117] To tune these parameters and the overall efficiency of the catalyst, a wide variety of metals and support materials have been tested for the photothermal reduction of CO_2 (Tables 1–3).

3.2.1. Strongly plasmonic metal nanoparticle based catalysts

(Strongly) plasmonic metals can show LSPR oscillation in the solar spectrum and are therefore widely used as nanoparticles on solar CO_2 reduction catalysts.[15,58,118] This is illustrated by the use of copper in combination with platinum nanoparticles on reduced (blue) titania, to promote CO_2 reduction. The introduction of copper significantly enhanced CO_2 adsorption while the copper nanoparticles readily accepted electron transfer from the platinum on the blue titania.[119] This was exemplified by the relative performance differences between the two different hierarchical bimetallic nanoparticle structures. The hierarchical order of nanoparticle deposition of platinum first and copper second resulted in the highest productivity increase compared to their previous work. In further research, the authors investigated a Z-scheme heterojunction of reduced TiO_2–Cu_2O photocatalyst. Although it had lower productivity than their previous work, the catalyst demonstrated high stability while utilizing a non-noble metal co-catalyst, making it a promising next step in the development of artificial photosynthesis.[120]

Zhou, Sun, Ozin, and co-workers investigated another non-noble metal based catalyst for the production of carbon monoxide from carbon dioxide and hydrogen. The catalyst was composed of Cu_2O nanocubes with mixed oxidation states.[121] The nanocubes allowed for heterolysis of hydrogen and adsorption of carbon dioxide under mild conditions. The stability of the catalyst was improved by modifying the surface of Cu_2O with a mixed valence surface frustrated Lewis pair. Alternatively, copper-substituted hydroxyapatite can be used as non-noble metal catalyst in the RWGS reaction. A strong photothermal effect was found for copper nanoparticles, enhancing the production of CO.[122]

Gold nanoparticles on TiO_2 did also show increased production of carbon monoxide upon light irradiation.[123,124] Molina *et al.* discuss the photothermal and photochemical contribution of the light.[123] The light-driven process obtained higher activity and selectivity in comparison to thermal reference experiments. Previous research based on experimental and theoretical analysis supported that the reaction was promoted by a synergistic contribution of (photo)thermal and photochemical processes.[125,126] Upadhye *et al.* ruled out localized heating effects based on reported literature[127] and the apparent activation energies found.[124] Here, the increase in productivity was predominantly attributed to a reduction in inhibition due to surface coverage of adsorbed species, which could be caused by either hot electrons or intense electromagnetic fields around the gold nanoparticles.

Gold nanoparticles can also be used on carbon nitride to increase the photocatalytic activity.[128] This is because the formation of a Schottky barrier between the semiconductor material and the metal nanoparticle facilitates the separation of electron-hole pairs. Furthermore, surface plasmon resonance effects could enable the formation of visible light excited electrons. The separated electrons could then be utilized in the process of reducing CO_2 to CO and CH_4. Meanwhile, the holes in the valence band of the carbon nitride could oxidize H_2O to produce O_2 and H^+. Other modifications can be made to the

© 2023 The Authors. ChemSusChem published by Wiley-VCH GmbH

1864564x, 2024, 4, Downloaded from https://chemistry-europe.onlinelibrary.wiley.com/doi/10.1002/cssc.202301405 by Uva Universiteitsbibliotheek, Wiley Online Library on [02/05/2024]. See the Terms and Conditions (https://onlinelibrary.wiley.com/terms-and-conditions) on Wiley Online Library for rules of use; OA articles are governed by the applicable Creative Commons License

carbon nitride semiconductor catalyst, as carbon nanotubes (CNTs) can for example be introduced along with copper nanoparticles at the surface of the g-C_3N_4.[129]

3.2.2. Weakly plasmonic metal nanoparticle based catalysts

Kim *et al.* studied and compared a variety of metal (e.g., platinum, copper, rhodium, nickel and ruthenium) nanoparticles on a silica support.[40] The choice of metal greatly influenced the product distribution, with some catalysts showing high selectivity towards either methane or carbon monoxide. The ruthenium nanoparticles demonstrated significant enhancement in methane productivity upon irradiation, claimed to be due to the formation of hot electrons. In contrast to ruthenium, platinum nanoparticles showed the highest activity towards carbon monoxide, for temperatures above 300 °C. Formation of carbon monoxide at lower temperatures was observed for palladium and platinum on WO_3 based catalysts.[130,131] The high conversion and selectivity for palladium nanocrystal decorated WO_3 nanowires were attributed to the formation of hydrogen tungsten bronzes (H_yWO_{3-x}), containing Brønsted protons, excess electrons and oxygen vacancies in its lattice.[130] Performance of this type of catalyst could be further increased by coating copper atoms onto the surface.[132] These examples illustrate the use of solar light with other (weakly plasmonic) metal nanostructures in combination with, or in comparison to, other metals described before.[133,134]

Further investigation of rhodium nanoparticles has been performed by Song, Wang, and co-workers, which used titanium dioxide as support material.[135] Mechanistic studies based on X-ray photoelectron spectroscopy (XPS) measurements indicated that hot electrons were generated upon light irradiation, which were then transferred to the TiO_2 support. The loading of the metal was also important for the overall catalytic activity, with high loadings leading to large nanoparticles and reduced activity. The catalytic mechanism was investigated using a variety of experiments, including *in situ* Diffuse Reflectance Infrared Fourier Transform Spectroscopy (DRIFTS), leading to a proposed mechanism (see Figure 4). The accumulation of hot electrons on the TiO_2 and an elevated local temperature could improve the overall production of carbon monoxide.

The use of rhodium as metal species has been shown to form carbon monoxide. For the formation of methane, nickel and ruthenium-based catalysts can be used as these metals show high selectivity towards this compound. Several support materials, including strontium titanate, Nb_2C, Ti_3C_2 and Al_2O_3, have been suggested to be used and evaluated in combination with these metals.[136–141] The support can prevent the sintering of the metal nanoparticles and increase the stability of the catalyst.[142] The interest in nickel and ruthenium lies in their increased affinity for CO_2 and potential intermediates, which leads to higher selectivity towards methane formation.[143] In order to improve the availability of CO_2 at the active site, Layered Double Hydroxides (LDH) have been identified as another efficient support for nickel and ruthenium nanoparticles in CO_2 methanation.[144,145] The abundant OH groups at the surface of the supports facilitate both the adsorption and activation of CO_2.

To increase the performance of another nickel CO_2 methanation catalyst, Scott, Lovell and co-workers utilized a plasma treatment to create a defective titania support.[146] Nickel nanoparticles were subsequently deposited on the support, and different combinations of reduction steps and plasma passivation treatments were studied. The authors reported that the plasma treatment resulted in extra oxygen vacancies, which increased the interaction between CO_2 and the support, leading to improved performance of the catalytic system. The use of a support material with inherent oxygen vacancies, like CeO_2, has also been shown to achieve good performances when combined with cobalt or nickel nanoparticles, exemplifying the benefit of these vacancies.[147]

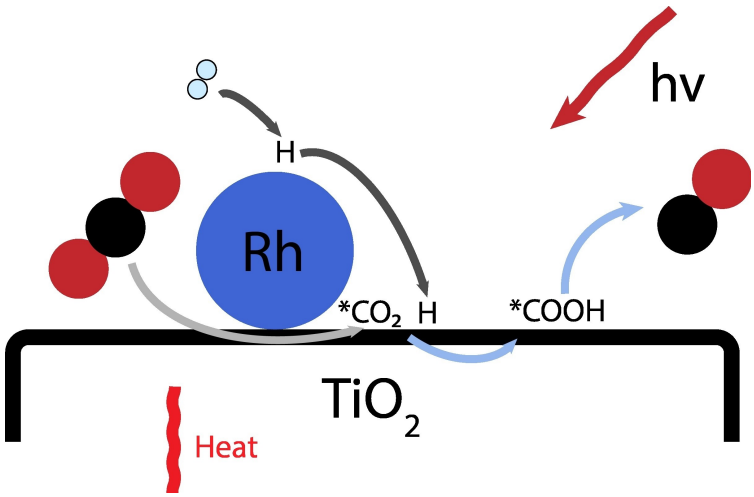

Figure 4. Proposed reaction mechanism for photo-assisted CO_2 hydrogenation reaction process over Rh/TiO_2. Adapted with permission from ref [135]. Copyright 2022 American Chemical Society.

© 2023 The Authors. ChemSusChem published by Wiley-VCH GmbH

1864564x, 2024, 4, Downloaded from https://chemistry-europe.onlinelibrary.wiley.com/doi/10.1002/cssc.202301405 by Uva Universiteitsbibliotheek, Wiley Online Library on [02/05/2024]. See the Terms and Conditions (https://onlinelibrary.wiley.com/terms-and-conditions) on Wiley Online Library for rules of use; OA articles are governed by the applicable Creative Commons License

The use of another cobalt based methanation catalysts has been evaluated using titanium dioxide combined with lanthanum oxide as support material.[148] Catalysts with various La_2O_3 to TiO_2 support ratios were synthesized and tested with cobalt nanoparticles. It was found that having up to 10% of La_2O_3 in the support improved the activity of the catalyst. This is because the basicity of La_2O_3 facilitates CO_2 coordination and $HCOO^•$ formation at the surface of the catalyst. Further insight in the effect of the support was obtained by Ye and co-workers, who investigated ruthenium based catalysts on different supports.[149] Activity and selectivity were largely influenced by the support material. Eventually, high methane production was achieved for natural halloysite nanotubes-supported Ru nanoparticles.

The selectivity and activity of the transformation can be further tuned by engineering the metallic site of the catalyst. Incorporating an oxophilic metal in the catalyst can improve its activity, as demonstrated by Huber *et al.*[150] In their study, a silica-supported platinum RWGS catalyst was used with molybdenum incorporated on the nanoparticles. The incorporation of molybdenum resulted in a significant improvement in the carbon dioxide conversion rate compared to the catalysts using solely molybdenum or platinum on the silica support, as the oxophilic metal could alleviate catalyst poisoning by carbon monoxide. Further tuning of the metallic site can be achieved by the integration of nickel into a phosphorous lattice, leading to highly dispersed nickel nanoclusters.[151] This combination disfavors strong carbon monoxide bonding, adding to the high selectivity of the catalyst.

In a recent report, Ozin and co-workers screened various combinations of palladium nanocrystals and Nb_2O_5 as active support.[152] They found that reducing the size of the nanocrystals of palladium at the surface of Nb_2O_5 nanorods unlocked an enhanced production of carbon monoxide with higher selectivity. This was explained through DFT analysis using a donor-electron acceptor interaction model, which explained the shift in palladium binding energy. With a smaller crystal size, electrons can be efficiently transferred to the Nb_2O_5 support, creating a partially positive charge on the palladium. This partial charge can affect the binding of the gas. With a larger nanocrystal, less charge transfer would occur, contributing to further reduction of carbon monoxide towards methane (see Figure 5).

In catalyst synthesis, metal-organic frameworks (MOFs) show potential as template and precursor, which was illustrated by Ye and co-workers.[153] Here, an iron-containing MOF (MIL-101) was used to obtain iron nanoparticles, coated with an ultrathin carbon layer. A thermal effect in the RWGS reaction was found for the visible and infrared part of the spectrum. The ultraviolet part generated energetic electrons mediated by the excitation of surface plasmons. DFT calculations supported the high selectivity to CO and showed weak physical adsorption of CO on the coated iron nanoparticle. The use of MOFs has also been shown in the Sabatier reaction, where the MOF UiO-66 was combined with iridium nanoparticles.[154] The iridium nanoparticles enclosed in the MOF material could efficiently facilitate the separation and the transfer of charge carriers in the UiO-66 material, which led to a good methane production.

3.3. Catalyst evaluation

A large variety of catalysts, based on different materials, have been prepared and tested in the continuous solar-driven reduction of CO_2 to either CO or CH_4, an overview of the catalysts can be found in Tables 1–3. As illustrated, the synergy between support and metal species is key to obtain optimal solar light utilization and selective product formation. Still, the overall efficiency can be increased, and more research is required to obtain catalysts with full solar spectrum absorbance

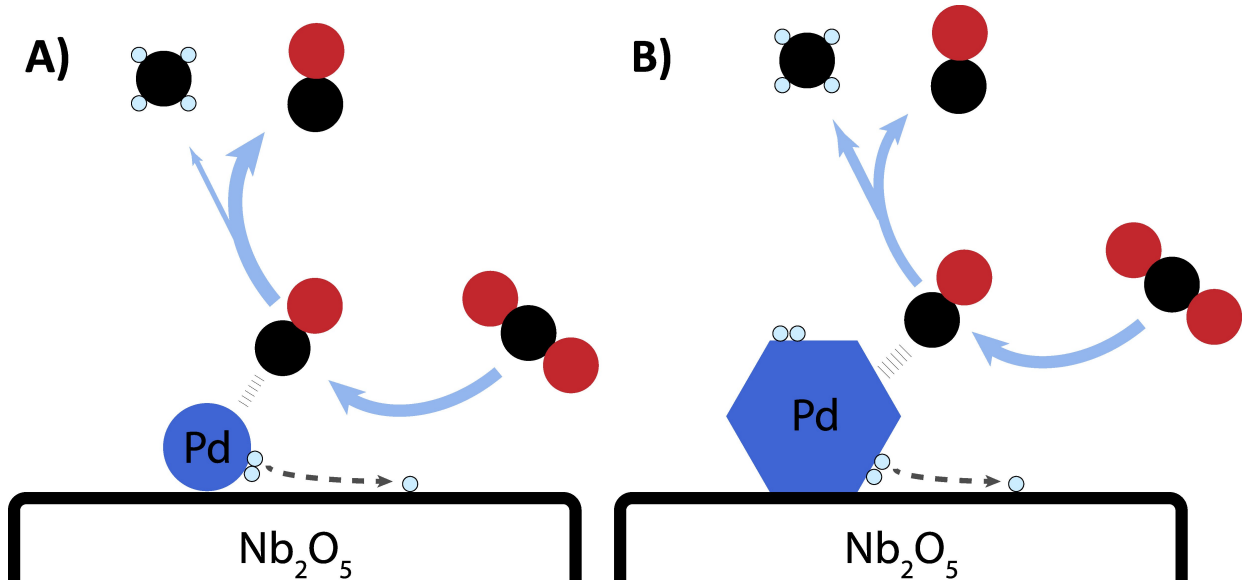

Figure 5. These schematic illustrations depict the influence of the size of the Pd nanocrystals on the selectivity of the CO_2 reduction. A) Small Pd nanocrystal. B) Large Pd nanocrystal leading to an increased CH_4 production. Adapted with permission from ref [152]. Copyright 2017 John Wiley and Sons.

© 2023 The Authors. ChemSusChem published by Wiley-VCH GmbH

1864564x, 2024, 4, Downloaded from https://chemistry-europe.onlinelibrary.wiley.com/doi/10.1002/cssc.202301405 by Uva Universiteitsbibliotheek, Wiley Online Library on [02/05/2024]. See the Terms and Conditions (https://onlinelibrary.wiley.com/terms-and-conditions) on Wiley Online Library for rules of use; OA articles are governed by the applicable Creative Commons License

and low energy losses. Plasmonic coupling and collective thermal effects may also significantly contribute to performance enhancement.[65,155,156] High activity and selectivity can decrease the amount of catalyst needed and ease the separation in downstream processes. Other factors as safety, price and availability of the catalysts cannot be overlooked in the use of these materials in scaled up applications. These conditions imply the use of non-noble and non-toxic material with excellent photothermal properties. As illustrated, many CO_2 reduction catalysts use scarce or costly metals to enhance the performance, where also several promising abundant and low-cost options are presented. Other desirable properties for scale-up include long term stability, which requires testing in an operating system for a sustainable amount of time. Loss of activity over time can be detrimental in the application of such a catalyst in industry. Moreover, heat transfer properties of the catalyst should not be overlooked, where temperature gradients in the catalyst bed should be controllable and heat losses to the environment minimized. Efficient utilization of the catalyst does also heavily rely on the identification of the most favorable operating conditions. Overall, several challenges remain in the development of solar-driven CO_2 reduction catalyst.

4. Flow chemistry and continuous photoreactors

Traditionally, synthesized catalysts are investigated in batch systems to assess the various parameters affecting the reaction. Loading a reactor with reagents and the catalysts, exposing this system to the reaction conditions for a defined amount of time before stopping, purifying, and analyzing the reaction mixture is a straightforward approach for most processes. However, for gas reactions, this process has several disadvantages, with perhaps the most significant being the difficulty of scaling up such a batch system. Scaling up pressurized vessels not only poses safety concerns but also allows for temperature gradients inside reactors more easily. As the dimensions increase, it becomes more challenging to achieve well-distributed irradiation of the catalyst, which is crucial for optimal reactor performance.[157,158] For light-driven reactions the catalyst will be used in an inefficient manner when using bulky reactors with thick catalyst beds due to the limited light penetration depth (typically less than 1 mm).[123] Furthermore, batch reactors can induce selectivity issues since products can accumulate inside the reactor, making them more susceptible to undesired sequential reactions.[159] This product accumulation within a batch system limits their suitability for extended operation and industrial applications, as well as further complicating the fair comparison of catalyst performance.[86]

Continuous-flow reactors, with high surface area to volume ratios and excellent heat transfer properties, are a suitable alternative to batch reactors to perform solar-driven CO_2 conversion.[160–164] In fact, it has been determined that flow reactors require a much lower CO_2 conversion rate to achieve net CO_2 reduction using sunlight as the energy source.[14] From an industrial standpoint, a continuous stream of CO_2 that varies in both volumetric quantity and composition can be encountered. In this case, continuous reduction of carbon dioxide with increased control would be more desirable than a batch-type approach. Moreover, continuous-flow reactors can be employed using a numbering up and/or sizing up strategy, which involves replicating identical reaction units in parallel and increasing the size of a single reactor unit, respectively.[165] These forms of scale-up enables straightforward tailoring of the size of the process to each CO_2 (point) source.

Small dimensions of flow channels allow for efficient use of the catalyst, as the light penetration depth is usually limited for heterogeneous catalysts.[166–168] Temperature gradients in the catalyst bed that arise from one sided illumination should be controllable, measured and accounted for in the design of the system.[66,72,169,170] Predictions on the temperature gradient in the catalyst bed and close surroundings can be made by the introduction of temperature sensors in the catalyst bed and simulations. These sensors should be small compared to the thickness of the catalyst bed to allow positioning of multiple sensors for monitoring the temperature gradient and to facilitate good thermal contact between the catalyst powder and the sensor. Furthermore, they should not suffer from photothermal heating and have minimum impact on the light distribution inside the catalyst bed. An example of suited temperature sensors is a fiber Bragg based-fiber optic sensor.[72] Temperature gradients are also expected to be present in continuous reactors, due to the low thermal conductivity of catalyst powders.[171] Still, a part of the heat is removed by convection, depending on the conditions, which should be taken into consideration.[172]

While scientific interest in flow processes keeps on growing, gaining a comprehensive understanding of the factors that contribute to system performance is challenging due to the vast differences in both experimental conditions and reporting. For example, the choice of catalyst, reactor type, irradiation, and measurement techniques can greatly influence the reported results. Furthermore, the lack of standardization in experimental protocols and reporting makes it difficult to compare the performance of different systems in a meaningful way. Therefore, it is important to carefully consider and report all relevant experimental conditions and precise setup (e.g., light source and materials used) when evaluating the performance of a photothermal system for CO_2 reduction. This will enable better comparison between systems and facilitate the development of more efficient and sustainable CO_2 conversion technologies.

Various approaches to continuous photoreactor design have been proposed, including optical fiber, double-skin sheet, fluidized bed, and annular reactors.[173–176] The transparent part should be designed to allow for homogeneous irradiation of the catalyst bed and its material should have minimal absorption in the solar spectrum to minimize energy losses. Reflection losses from the surface of the reactor should be minimized, for example, by applying anti-reflective coatings or surface treatments. Light sources can be used to mimic solar

© 2023 The Authors. ChemSusChem published by Wiley-VCH GmbH

1864564x, 2024, 4, Downloaded from https://chemistry-europe.onlinelibrary.wiley.com/doi/10.1002/cssc.202301405 by Uva Universiteitsbibliotheek, Wiley Online Library on [02/05/2024]. See the Terms and Conditions (https://onlinelibrary.wiley.com/terms-and-conditions) on Wiley Online Library for rules of use; OA articles are governed by the applicable Creative Commons License

irradiation and ease the testing of catalysts in a laboratory environment without requiring field experiments. A variety of light sources with a spectrum similar to the solar spectrum exist, consisting of, amongst others, LEDs, xenon light sources and metal halide lamps.[177] The light source's positioning and the distance between the light source and the catalytic bed affect the (homogeneity of the) light intensity and should therefore be carefully chosen and reported.[178,179]

For the photothermal conversion of CO_2 unconcentrated solar irradiation might not provide sufficient energy to obtain the desired activity. Therefore, concentrated (solar) light can be employed to increase the light intensity at the reactor, which can, for example, be determined with radiometry.[180,181] The use of light sensors could allow for a real time feedback system to ensure optimized production at different solar light intensities.[182] Several approaches to collect and concentrate light can be applied, where most systems use glass mirrors due to their high reflectivity. Examples of concentrating solar power technologies are parabolic trough collectors, parabolic dish systems and linear Fresnel reflectors.[158,161,183,184] Solar light concentrators have been applied before in water purification, water splitting and thermochemical processes, and its use can be extended to photothermal CO_2 reduction in batch or continuous-flow.[185–195] Depending on the concentrator configuration, high temperatures can be obtained, which should be matched with the requirements of the catalyst.[185,193]

The use of these concentrators in CO_2 reduction was illustrated by Kandy and Gaikar, where this technology was used to boost alcohol production.[196] Fresnel lenses (Figure 6C) have been employed as solar light concentrators in batch and continuous-flow photothermal reduction of CO_2 and allow for the use of concentrated solar light in a cost effective manner.[197–201] Different configurations to concentrate solar light on a reactor are illustrated in Figure 6. Depending on the light concentrating system, the solar light harvesting ability can be increased by solar tracking.[202,203] The light flux profile, and thus the type of concentrator, and reactor geometry should be adapted to one another to make efficient use of the incident solar light. Furthermore, the use of concentrated light does pose new challenges for uniform catalyst irradiation.[204–206]

The deposition and placement of the catalyst in the reactor does not only influence the homogeneity of the light intensity, but also significantly affects the production, through mass transfer properties, pressure drop, and the homogeneity of the temperature.[207–210] Reactors for photothermal CO_2 conversion can be classified as fixed bed or structured reactors.[211] In contrast to fixed bed reactors, structured reactors usually have a unique structure presenting numerous channels and a large surface area. Commercially available fixed bed reactors (e.g., Harrick scientific[212]) have the advantage of being well-characterized, ensuring higher inter-laboratory reproducibility of the obtained experimental results. However, a homemade or custom-made fixed bed photoreactor can also be constructed (e.g., to minimize the costs). Tubular or annular packed bed reactors are relatively straightforward to construct, illuminate, and operate, which adds to their frequent use in similar systems. Figure 7 illustrates different types of catalyst placement in a photoreactor that can be encountered in heterogeneous catalysis.

One possible fixed bed reactor design uses an additional support for the catalyst, which can be introduced into the reactor. The reactor design should ensure that the catalyst remains contained within it (i.e., no leaching of the catalyst should occur). This deposition method is frequently used in continuous-flow testing, as also stands out from Tables 1–3, as it can be easily applied in different reactor designs. The use of this type of fixed bed reactors allows for straightforward operation, fast parametric screening, and facile combination with commercially available solar simulators. A glass flow reactor was used for this type of catalyst immobilization (see Figure 8A and B). The reactor allowed for the evaluation of ruthenium nanoparticles on a LDH support.[145] The applicability of this fixed bed immobilization method is shown by Zhang and co-workers, which use a stainless steel reactor with a quartz window (Figure 8C and D) to test the performance of a series of nickel based catalysts.[144]

Additionally, if external heating is required, a heating mantel can be used, as illustrated by the in-house developed photoreactor depicted in Figure 9A and B.[213] The use of an external heating source should allow for a uniform irradiation of

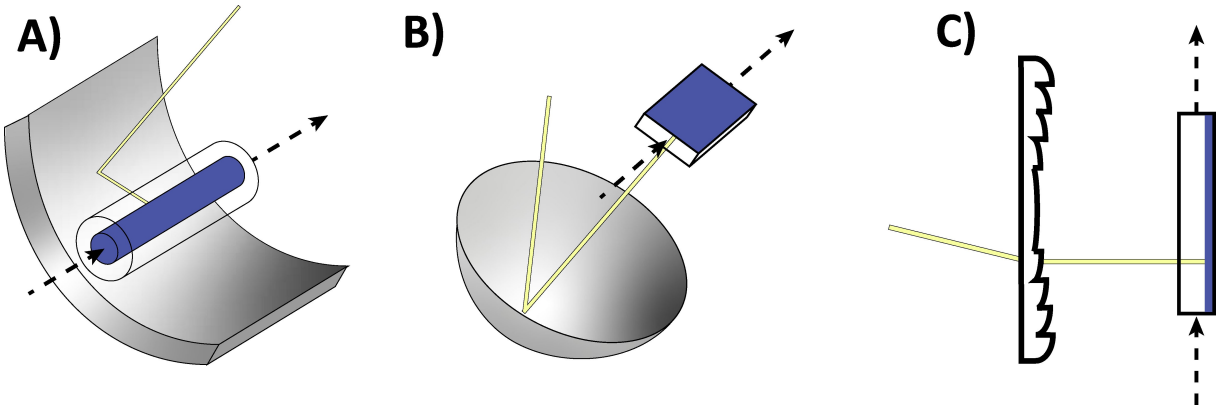

Figure 6. Schematic of different (solar) light concentrators: A) parabolic trough collector B) Parabolic dish. C) Fresnel lens. Shown in combination with a continuous-flow reactor. A) & B) Adapted with permission from ref [193]. Copyright 2014 Elsevier.

© 2023 The Authors. ChemSusChem published by Wiley-VCH GmbH

1864564x, 2024, 4, Downloaded from https://chemistry-europe.onlinelibrary.wiley.com/doi/10.1002/cssc.202301405 by Uva Universiteitsbibliotheek, Wiley Online Library on [02/05/2024]. See the Terms and Conditions (https://onlinelibrary.wiley.com/terms-and-conditions) on Wiley Online Library for rules of use; OA articles are governed by the applicable Creative Commons License

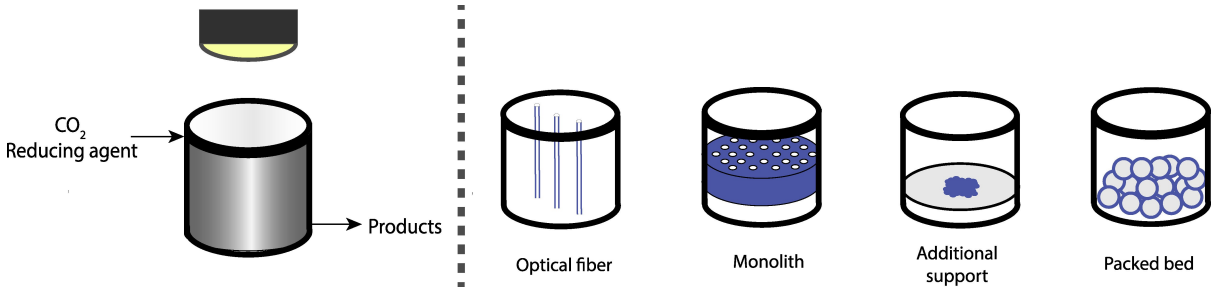

Figure 7. Left: Schematic set-up of a continuous flow reactor for CO_2 reduction with irradiation source above the reactor chamber. Right: Examples of different types of fixed bed or structured catalyst deposition.

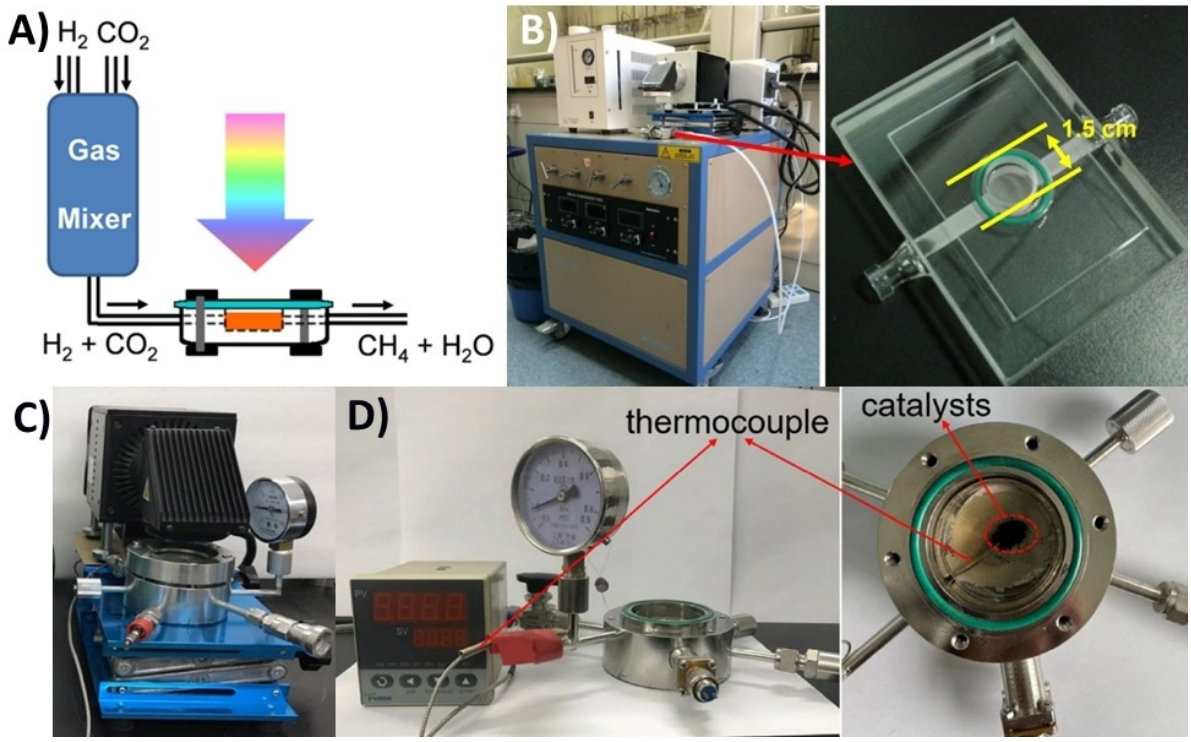

Figure 8. A) Schematic of the flow photoreactor setup. B) Actual flow photoreactor setup with the solar simulator and close up on the photoreactor. Adapted with permission from ref [145]. Copyright 2017 John Wiley and Sons. C) Photoreactor consisting of a stainless reaction chamber with a quartz window, with the light source. D) Placement of the thermocouple and catalyst inside the reactor. Adapted with permission from ref [144]. Copyright 2021 Spinger Nature.

the catalyst bed. This flow reactor was validated by testing commercially available catalysts (Ni-Al_2O_3/SiO_2), loaded on the top of a fritted glass filter. The desired temperature could be set, while an optic fiber guided the simulated solar light towards the catalyst surface. The researchers discussed the effect of temperature and irradiation wavelength by using cut-off filters to assess the conversion towards methane. Similarly, Bueno-Alejo *et al.* used the same catalyst in a flow system that combined high power LEDs with a fixed bed reactor (see Figure 9C).[214] With their reactor system, light sources could be exchanged and compared. After screening various wavelengths, the authors concluded that irradiation at 460 nm led to a combined photothermal and photocatalytic response resulting in a boost in the catalyst productivity.

Glass beads can also be used as additional support. The catalyst can be deposited upon the glass beads, which are then randomly distributed throughout the reactor in a packed bed design. The size of the beads and thickness of the catalyst layer greatly influence the mass transfer properties, light penetration, and pressure drop of the reactor, which has been extensively studied.[215–217] The catalyst can also be coated as a film on an additional support or directly onto the reactor wall, which can profoundly decrease pressure drop effects compared to packed bed reactors.[218] Optical fibers can act as support for the coating of the catalyst. Typically, an optical fiber consists of a core and cladding to achieve total internal reflection. However, in order for the catalyst to absorb photons, light needs to leak along the length of the fiber.[219] This light leakage can be achieved, for example, by selectively etching the cladding, after which the catalyst is applied to the fiber. In optical fiber photoreactor design, light travels along the fiber leading to a drastic increase in available relative irradiated area.[220]

© 2023 The Authors. ChemSusChem published by Wiley-VCH GmbH

1864564x, 2024, 4, Downloaded from https://chemistry-europe.onlinelibrary.wiley.com/doi/10.1002/cssc.202301405 by Uva Universiteitsbibliotheek, Wiley Online Library on [02/05/2024]. See the Terms and Conditions (https://onlinelibrary.wiley.com/terms-and-conditions) on Wiley Online Library for rules of use; OA articles are governed by the applicable Creative Commons License

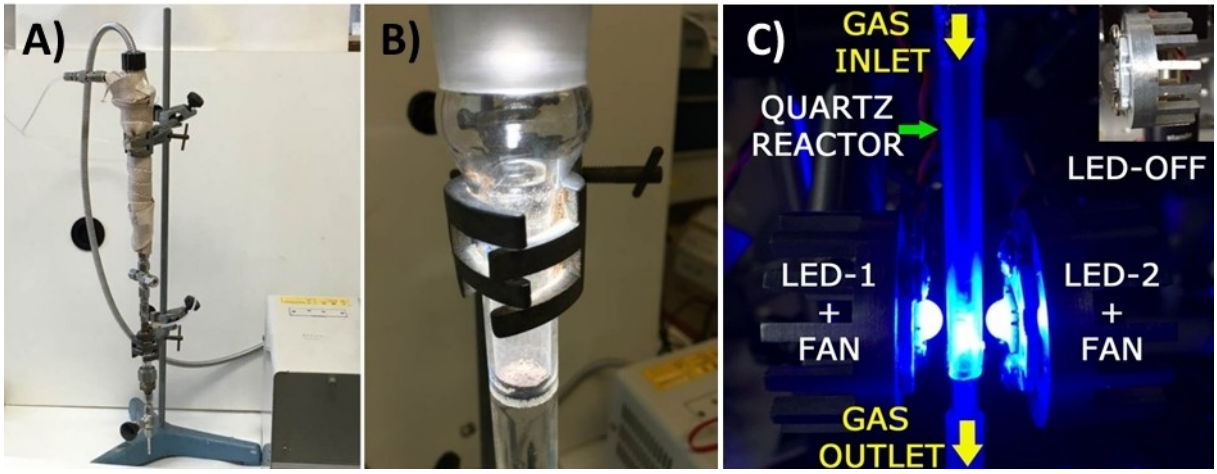

Figure 9. A) Flow photoreactor setup with a heating mantle. B) Close-up of the irradiated catalyst deposed on a glass frit. C) Flow photoreactor setup with interchangeable LEDs for wavelength screening. (A) and (B) reprinted with permission from ref [213]. Copyright 2017 Royal Society of Chemistry. (C) Adapted with permission from ref [214]. Copyright 2020 Elsevier.

Wu *et al.* used an optical fiber photoreactor (Figure 10A and B)[221] for the photoreduction of CO_2 using concentrated solar light.[222] The optical fibers, with their polymer cladding removed by calcination, were coated with a metal-doped TiO_2—SiO_2 sol-gel, where the doped iron contributes to enhanced visible light absorption. Methane was selectively produced under concentrated natural sunlight irradiation through the quartz window. In another experiment, Wu *et al.* dip-coated the optical fibers with dye-sensitized metal-doped TiO_2.[223] With a high-intensity artificial light source, both methane and ethylene were produced. However, the setup using natural concentrated solar light selectively produced methane, most likely due to its significantly lower light intensity.

One of the limitations of optical fiber reactor types is the relatively small thickness of the fibers, which limits the total available catalytic surface area and active reactor volume. To alleviate this issue, Wu *et al.* proposed a honeycomb-structured monolith reactor as a next step towards scale-up.[224] A monolith structure consists of a regular or irregular network of meso- and microporous channels,[226] which tend to have efficient mass

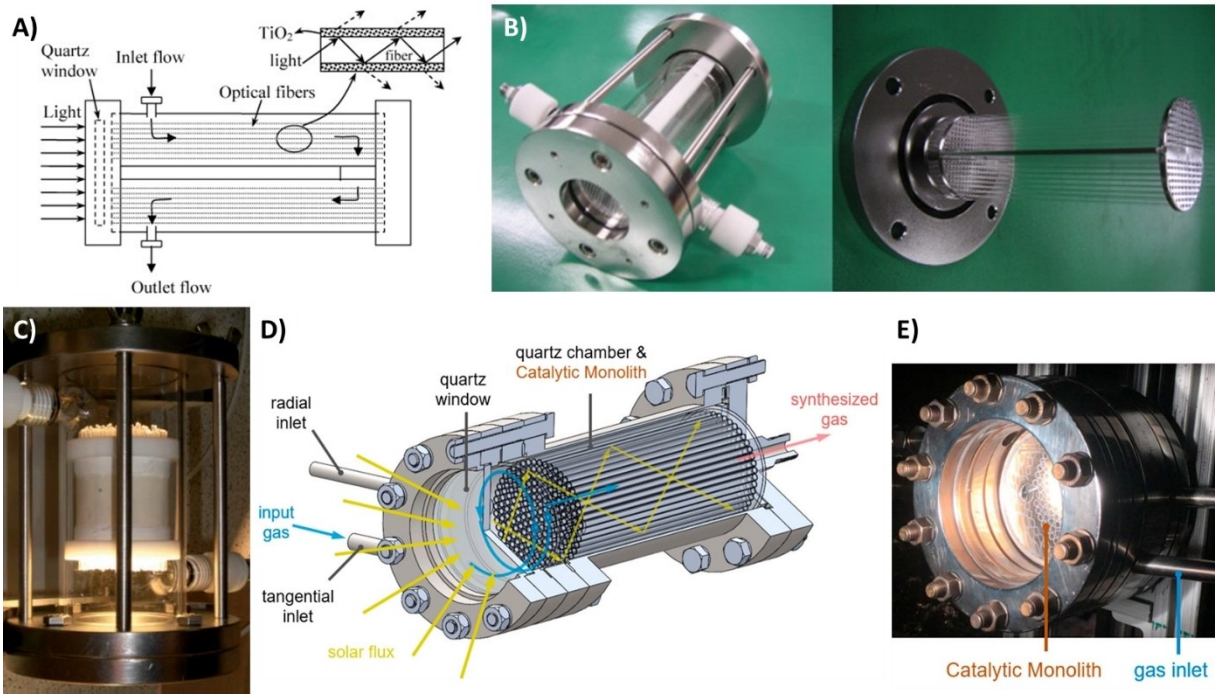

Figure 10. The optical fiber reactor schematically (A) and with pictures of the built reactor (B). C) The internally illuminated monolith reactor in operation. The tubular monolith reactor schematically (D) and in operation (E). (A) and (B) adapted with permission from ref [221], copyright 2008 Elsevier, (C) adapted with permission from ref [224], copyright 2011 Royal Society of Chemistry, and (D) and (E) adapted with permission from ref [225]. Copyright 2019 Elsevier.

© 2023 The Authors. ChemSusChem published by Wiley-VCH GmbH

1864564x, 2024, 4, Downloaded from https://chemistry-europe.onlinelibrary.wiley.com/doi/10.1002/cssc.202301405 by Uva Universiteitsbibliotheek, Wiley Online Library on [02/05/2024]. See the Terms and Conditions (https://onlinelibrary.wiley.com/terms-and-conditions) on Wiley Online Library for rules of use; OA articles are governed by the applicable Creative Commons License

transfer, a large geometric surface area, and allow for high flow rates without a significant pressure drop relative to packed bed systems.[226,227] However, for photochemical purposes, the poor light penetration within these systems limits their use. The conceptual reactor design used was built upon the previous optical fiber reactor design. In this design, the fibers were inserted within the monolith structure, which allowed for irradiation of the internal monolith surface (Figure 10C). Since the function of optical fibers is normally to transport light along the fiber by total internal reflection, the outer surface of the optical fibers was carved to produce sideways irradiation. The ends of the fibers were treated with aluminum to provide back reflection into the system.

The internally illuminated monolith reactor concept was used for the continuous production of methanol, methane and acetaldehyde, using different catalyst loadings on the monolith.[228] The potential of a solar monolith reactor was also investigated by Trelles and co-workers, but the design approach was significantly different from the inserted optic fiber concept.[225] This reactor design similarly used a cylindrical vessel with irradiation through a quartz window, but the monolith was constructed by bundling individual quartz tubes together (Figure 10D and E). These tubes were dip-coated with Cu/TiO_2 and placed within the reactor. Experiments were also performed with zirconia foam disks coated with the same catalyst, because of their abundance of available surface area, but due to their optical thickness, the light could not penetrate the full reactor volume. The synergistic effect of an increase in both light intensity and catalytic surface temperature was investigated. Additionally, a computational fluid dynamics (CFD) model was developed, experimentally validated and used to fully describe fluid flow as well as heat-, mass-, and radiation-transport within the system for varying irradiation intensities of the light source.

Similarly to optical fiber reactors, catalyst irradiation can be improved by the use of an annular glass cylindrical rod photoreactor.[229] In this setup, defect-laden indium oxide is coated on a waveguide to enhance carbon monoxide production from carbon dioxide and hydrogen. As shown in Figure 11, the light distribution along the length of the waveguide increased the optical pathlength of the weakly absorptive green and yellow wavelengths. For blue light, the intensity decreases with the length of the rod, indicating that the coating partially absorbs the light as it is internally reflected. In addition to its light absorption properties, the catalyst showed persistent photoconductivity behavior, continuing to produce carbon monoxide even after turning off the illumination.

Li *et al.* show in a unique approach the direct use of weak solar irradiation (1 kW/m^2) by using a selective light absorber that can generate temperatures up to 288 °C without an external heating system in a quartz tube reactor.[230] This increased local temperature combined with ultrathin amorphous Y_2O_3 nanosheets and confined single nickel atoms exhibited an increased activity for CO_2 methanation. Use of concentrated solar light was shown in a reactor by combining a compound parabolic concentrator (CPC) with an annular reactor (Figure 12A).[175] This reactor type has been used to perform the RWGS with In_2O_{3-x} $(OH)_y$ nanorods coated on a substrate. The system's stability was demonstrated through sustained operation exceeding 70 hours with simulated solar light irradiation. In a similar annular reactor combined with a CPC, a photocatalytic foam was evaluated in order to increase carbon monoxide production.[231] In this application, $In_2O_{3-x}(OH)_y$-coated nickel foam can improve mass transfer efficiency, in comparison to coating the catalyst as a film (Figure 12B and C). The product selectivity differed from previous reports, which was attributed to the introduction of the oxidized nickel foam.

Different approaches for continuous reactors to convert CO_2 have been proposed. Solar light harvesting ability can be increased by the use of concentrators, which should irradiate the catalysts inside the (optically transparent) reactor. Testing catalysts with (concentrated) natural solar light has been shown by a few examples, but further experiments are required to prove the viability of the technique. Reactor design should include the handling of high temperatures and preferably elevated pressures. The homogeneously irradiated catalyst should make efficient use of the incident light and the reagents should be converted without encountering mass transfer limitations, while pushing towards the highest activity as possible. For the latter the influence of parameters on the system should be known, which can be determined experimentally and with simulations. As illustrated, the design of a photothermal system and the operation requires interdisciplinary expertise, including chemical engineering, computational chemistry, optics, material science and chemistry. Combining all these fields together is challenging but is required to develop

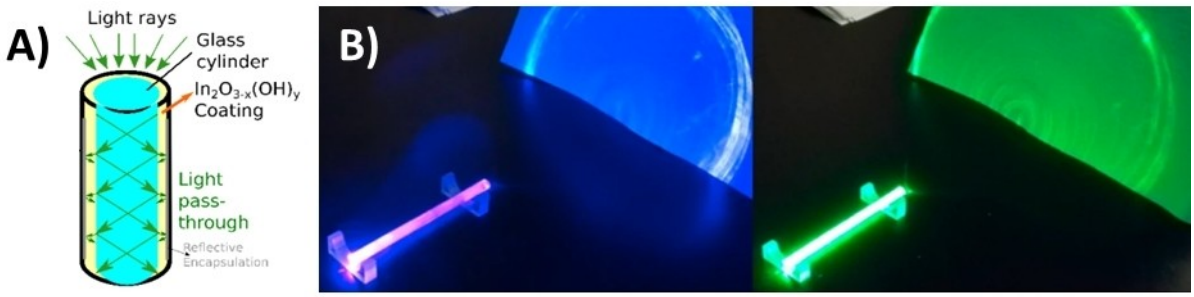

Figure 11. A) Schematic showing how light guiding distributes light throughout the coating. B) Waveguiding blue and green laser illumination at an angle of incidence of 60°. Adapted from ref [229], copyright 2021 Nature Publishing Group, licensed under CC BY 4.0.

© 2023 The Authors. ChemSusChem published by Wiley-VCH GmbH

1864564x, 2024, 4, Downloaded from https://chemistry-europe.onlinelibrary.wiley.com/doi/10.1002/cssc.202301405 by Uva Universiteitsbibliotheek, Wiley Online Library on [02/05/2024]. See the Terms and Conditions (https://onlinelibrary.wiley.com/terms-and-conditions) on Wiley Online Library for rules of use; OA articles are governed by the applicable Creative Commons License

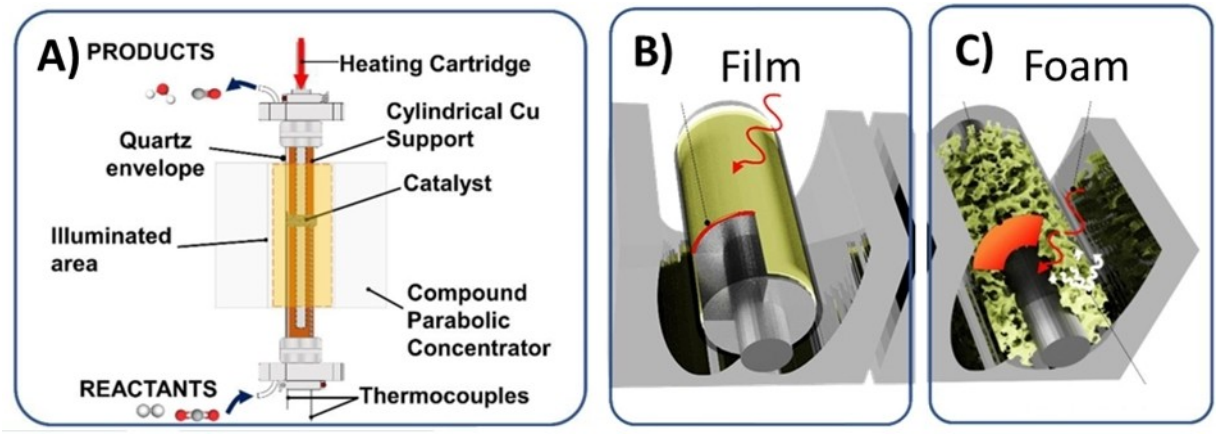

Figure 12. A) Scheme of the annular photoreactor with compound parabolic concentrator to conduct the photo- and thermal CO_2 hydrogenation. Graphical representation of different reactor configurations: thin film (B) and coated foam (C). Adapted with permission from ref [231]. Copyright 2022 Elsevier.

the most efficient systems possible. Future steps in this development of photothermal CO_2 conversion systems can include automation and optimization, which has gained significant attention in this and other fields and can increase the performance and economic attractivity of the technology. An issue to address is the conversion of CO_2 for low solar light intensities (e.g., at night, overcast weather). For example, artificial light can be used if production in the same system is desired under these conditions. The implementation of artificial light requires additional design and can be facilitated by the use of light sensors and automation of the system. Ideally, the light sources can be powered by green electricity.

5. Conclusions and Outlook

In this review, we have provided an overview of recent research efforts to develop technologies for converting CO_2 into value-added products. Specifically, we focused on the use of continuous-flow reactors in the photothermal production of methane and carbon monoxide, which can be performed with solar light as the ultimate green energy source.

Catalysts comprising a combination of a dielectric or semiconductive support and strongly or weakly plasmonic metallic nanoparticles are found to be good candidates in the solar-driven reduction of CO_2. A large part of the solar spectrum can potentially be used to synergistically contribute both thermally and photochemically to the process. The use of a broad range of the solar spectrum makes this type of catalyst more efficient than, for example, conventional metal oxide semiconductors, that only absorb highly energetic photons. Based on the evaluated catalysts (Tables 1–3), supported nickel and ruthenium nanoparticles show promising activity and selectivity in the formation of methane. For the production of carbon monoxide, altered indium oxide and non-noble metal nanoparticle catalysts show great potential.

We reviewed a selection of continuous-flow systems, which employ different approaches to increase light collection, catalyst irradiation, and production. The large variety of experimental set ups and methods for performance validation of photothermal catalysts stresses the importance of precise documentation of all relevant conditions to facilitate comparative analyses between different catalysts. Additionally, quantification of the thermal and non-thermal contributions of the light is important for fundamental understanding, rational optimization of the catalysts, and system design. Optimization of the catalyst layer thickness and metal loading, in combination with investigations to plasmonic coupling and collective thermal effects can further increase the performance of the catalyst.

Continuous-flow reactors have shown great promise in enabling the scaling up of CO_2 reduction and should enable industrial applications. A challenge to be met is the design of an efficient, fully integrated system, including light collection and concentration, catalyst deposition and heat management, which can only be achieved by close collaboration of research groups with expertise in chemistry, material science, chemical engineering, and optics. Further improvements in photothermal processes are expected with ongoing developments in the implementation of energy efficient artificial light sources, solar optics and process automation.

Overall, we emphasized the importance of developing sustainable and responsible solutions to address the global challenge of rising CO_2 concentrations. Experts from different fields have a critical role to play in this endeavor, and by working together, we can create a more sustainable and resilient future for ourselves and for generations to come.

Acknowledgements

This work was supported by European Union's Horizon research and innovation program (FlowPhotoChem, grant number 862453 and CATART, grant agreement number 101046836). The materials presented and views expressed here are the responsibility of the authors(s) only. The EU Commission takes no responsibility for any use made of the information set out.

© 2023 The Authors. ChemSusChem published by Wiley-VCH GmbH

18645564x, 2024, 4, Downloaded from https://chemistry-europe.onlinelibrary.wiley.com/doi/10.1002/cssc.202301405 by Uva Universiteitsbibliotheek, Wiley Online Library on [02/05/2024]. See the Terms and Conditions (https://onlinelibrary.wiley.com/terms-and-conditions) on Wiley Online Library for rules of use; OA articles are governed by the applicable Creative Commons License

Conflict of Interests

The authors declare no conflict of interest.

Keywords: carbon capture and utilization · photothermal catalysis · continuous-flow reactors · optics · system design

[1] J. M. West, J. Pearce, M. Bentham, P. Maul, *Eur. Environ.* **2005**, *15*, 250–259.
[2] T. L. Delworth, J. D. Mahlman, T. R. Knutson, *Clim. Change* **1999**, *43*, 369–386.
[3] W. D. Nordhaus, *The Climate Casino*, Yale University Press, **2015**.
[4] G. Rothenberg, *Sustain. Chem. Clim. Action* **2023**, *2*, 100012.
[5] B. Obama, *Science* **2017**, *355*, 126–129.
[6] R. J. Detz, B. van der Zwaan, *Energy Policy* **2019**, *133*, 110938.
[7] E. V. Kondratenko, G. Mul, J. Baltrusaitis, G. O. Larrazábal, J. Pérez-Ramírez, *Energy Environ. Sci.* **2013**, *6*, 3112.
[8] B. van der Zwaan, R. Detz, N. Meulendijks, P. Buskens, *Fuel* **2022**, *311*, 122547.
[9] P. Yue, Q. Fu, J. Li, X. Zhu, Q. Liao, *Green Chem.* **2022**, *24*, 2927–2936.
[10] P. Anastas, N. Eghbali, *Chem. Soc. Rev.* **2010**, *39*, 301–312.
[11] M. J. Mulvihill, E. S. Beach, J. B. Zimmerman, P. T. Anastas, *Annu. Rev. Environ. Res.* **2011**, *36*, 271–293.
[12] D. Dallinger, C. O. Kappe, *Curr. Opin. Green Sustain. Chem.* **2017**, *7*, 6–12.
[13] C. Wiles, P. Watts, *Green Chem.* **2012**, *14*, 38–54.
[14] S. Wang, A. A. Tountas, W. Pan, J. Zhao, L. He, W. Sun, D. Yang, G. A. Ozin, *Small* **2021**, *17*, 2007025.
[15] F. Zhang, Y.-H. H. Li, M.-Y. Y. Qi, Y. M. A. Yamada, M. Anpo, Z.-R. R. Tang, Y.-J. J. Xu, *Chem Catal.* **2021**, *1*, 272–297.
[16] X. Su, X. Yang, B. Zhao, Y. Huang, *J. Energy Chem.* **2017**, *26*, 854–867.
[17] P. Kaiser, R. B. Unde, C. Kern, A. Jess, *Chem. Ing. Tech.* **2013**, *85*, 489–499.
[18] C. Vogt, M. Monai, G. J. Kramer, B. M. Weckhuysen, *Nat. Catal.* **2019**, *2*, 188–197.
[19] T. Noël, S. L. Buchwald, *Chem. Soc. Rev.* **2011**, *40*, 5010–5029.
[20] I. Omae, *Coord. Chem. Rev.* **2011**, *255*, 139–160.
[21] Y. H. Choi, Y. J. Jang, H. Park, W. Y. Kim, Y. H. Lee, S. H. Choi, J. S. Lee, *Appl. Catal. B* **2017**, *202*, 605–610.
[22] J.-B. Peng, H.-Q. Geng, X.-F. Wu, *Chem* **2019**, *5*, 526–552.
[23] F. Raymenants, T. M. Masson, J. Sanjosé-Orduna, T. Noël, *Angew. Chem. Int. Ed.* **2023**, *62*, e202308563.
[24] S. Masoudi Soltani, A. Lahiri, H. Bahzad, P. Clough, M. Gorbounov, Y. Yan, *Carbon Capture Sci. Technol.* **2021**, *1*, 100003.
[25] A. A. Khan, M. Tahir, *J. CO2 Util.* **2019**, *29*, 205–239.
[26] S. Nitopi, E. Bertheussen, S. B. Scott, X. Liu, A. K. Engstfeld, S. Horch, B. Seger, I. E. L. Stephens, K. Chan, C. Hahn, J. K. Nørskov, T. F. Jaramillo, I. Chorkendorff, *Chem. Rev.* **2019**, *119*, 7610–7672.
[27] A. S. Agarwal, Y. Zhai, D. Hill, N. Sridhar, *ChemSusChem* **2011**, *4*, 1301–1310.
[28] G. Wang, J. Chen, Y. Ding, P. Cai, L. Yi, Y. Li, C. Tu, Y. Hou, Z. Wen, L. Dai, *Chem. Soc. Rev.* **2021**, *50*, 4993–5061.
[29] I. E. L. Stephens, K. Chan, A. Bagger, S. W. Boettcher, J. Bonin, E. Boutin, A. K. Buckley, R. Buonsanti, E. R. Cave, X. Chang, S. W. Chee, A. H. M. da Silva, P. de Luna, O. Einsle, B. Endrődi, M. Escudero-Escribano, J. V. Ferreira de Araujo, M. C. Figueiredo, C. Hahn, K. U. Hansen, S. Haussener, S. Hunegnaw, Z. Huo, Y. J. Hwang, C. Janáky, B. S. Jayathilake, F. Jiao, Z. P. Jovanov, P. Karimi, M. T. M. Koper, K. P. Kuhl, W. H. Lee, Z. Liang, X. Liu, S. Ma, M. Ma, H.-S. Oh, M. Robert, B. R. Cuenya, J. Rossmeisl, C. Roy, M. P. Ryan, E. H. Sargent, P. Sebastián-Pascual, B. Seger, L. Steier, P. Strasser, A. S. Varela, R. E. Vos, X. Wang, B. Xu, H. Yadegari, Y. Zhou, *J. Phys. Energy* **2022**, *4*, 042003.
[30] V. Kumaravel, J. Bartlett, S. C. Pillai, *ACS Energy Lett.* **2020**, *5*, 486–519.
[31] E. Boutin, M. Patel, E. Kecsenovity, S. Suter, C. Janáky, S. Haussener, *Adv. Energy Mater.* **2022**, *12*, 2200585.
[32] U. Ulmer, T. Dingle, P. N. Duchesne, R. H. Morris, A. Tavasoli, T. Wood, G. A. Ozin, *Nat. Commun.* **2019**, *10*, 3169.
[33] J. Zhou, H. Liu, H. Wang, *Chin. Chem. Lett.* **2023**, *34*, 107420.
[34] L. Zhou, J. M. P. Martirez, J. Finzel, C. Zhang, D. F. Swearer, S. Tian, H. Robatjazi, M. Lou, L. Dong, L. Henderson, P. Christopher, E. A. Carter, P. Nordlander, N. J. Halas, *Nat. Energy* **2020**, *5*, 61–70.
[35] M. Usman, W. M. A. Wan Daud, H. F. Abbas, *Renewable Sustainable Energy Rev.* **2015**, *45*, 710–744.
[36] Y. Zhou, R. Li, Z. Lv, J. Liu, H. Zhou, C. Xu, *Chin. J. Chem. Eng.* **2022**, *43*, 2–13.
[37] R. R. Beswick, A. M. Oliveira, Y. Yan, *ACS Energy Lett.* **2021**, *6*, 3167–3169.
[38] A. M. Oliveira, R. R. Beswick, Y. Yan, *Curr. Opin. Chem. Eng.* **2021**, *33*, 100701.
[39] C.-Y. Chen, J. Yu, V.-H. Nguyen, J. Wu, W.-H. Wang, K. Kočí, *Catalysts* **2017**, *7*, 63.
[40] C. Kim, S. Hyeon, J. Lee, W. D. Kim, D. C. Lee, J. Kim, H. Lee, *Nat. Commun.* **2018**, *9*, 1–8.
[41] Ž. Kovačič, B. Likozar, M. Huš, *ACS Catal.* **2020**, *10*, 14984–15007.
[42] S. Cai, J. Chen, Q. Li, H. Jia, *ACS Appl. Mater. Interfaces* **2021**, *13*, 14221–14229.
[43] X. Chen, S. Shen, L. Guo, S. S. Mao, *Chem. Rev.* **2010**, *110*, 6503–6570.
[44] Y. He, Y. Zhou, J. Feng, M. Xing, *Environ. Funct. Mater.* **2022**, *1*, 204–217.
[45] J. Low, L. Zhang, B. Zhu, Z. Liu, J. Yu, *ACS Sustainable Chem. Eng.* **2018**, *6*, 15653–15661.
[46] X. E. Cao, Y. Kaminer, T. Hong, P. Schein, T. Liu, T. Hanrath, D. Erickson, X. Elvis Cao, Y. Kaminer, T. Hong, P. Schein, T. Liu, T. Hanrath, D. Erickson, *iScience* **2020**, *23*, 101856.
[47] P. Riente, T. Noël, *Catal. Sci. Technol.* **2019**, *9*, 5186–5232.
[48] M. Ghoussoub, M. Xia, P. N. Duchesne, D. Segal, G. Ozin, *Energy Environ. Sci.* **2019**, *12*, 1122–1142.
[49] X. Wang, F. Wang, Y. Sang, H. Liu, X. Wang, F. Wang, Y. Sang, H. Liu, *Adv. Energy Mater.* **2017**, *7*, 1700473.
[50] H. Ge, Y. Kuwahara, K. Kusu, Z. Bian, H. Yamashita, *Appl. Catal. B* **2022**, *317*, 121734.
[51] S. Sarina, H.-Y. Zhu, Q. Xiao, E. Jaatinen, J. Jia, Y. Huang, Z. Zheng, H. Wu, *Angew. Chem.* **2014**, *126*, 2979–2984.
[52] I.-W. Un, Y. Sivan, *J. Appl. Phys.* **2019**, *126*, 173103, DOI 10.1063/1.5123629.
[53] S. Linic, P. Christopher, D. B. Ingram, *Nat. Mater.* **2011**, *10*, 911–921.
[54] L. Collado, A. Reynal, F. Fresno, M. Barawi, C. Escudero, V. Perez-Dieste, J. M. Coronado, D. P. Serrano, J. R. Durrant, V. A. de la Peña O'Shea, *Nat. Commun.* **2018**, *9*, 1–10.
[55] M. L. Brongersma, N. J. Halas, P. Nordlander, *Nat. Nanotechnol.* **2015**, *10*, 25–34.
[56] D. A. Panayotov, A. I. Frenkel, J. R. Morris, *ACS Energy Lett.* **2017**, *2*, 1223–1231.
[57] D. Mateo, J. L. Cerrillo, S. Durini, J. Gascon, *Chem. Soc. Rev.* **2021**, *50*, 2173–2210.
[58] S. Luo, X. Ren, H. Lin, H. Song, J. Ye, *Chem. Sci.* **2021**, *12*, 5701–5719.
[59] L. V. Besteiro, P. Yu, Z. Wang, A. W. Holleitner, G. V. Hartland, G. P. Wiederrecht, A. O. Govorov, *Nano Today* **2019**, *27*, 120–145.
[60] Q. Zhang, Z. Zuo, D. Ma, *Chem. Commun.* **2023**, *59*, 7704–7716.
[61] G. Baffou, R. Quidant, *Chem. Soc. Rev.* **2014**, *43*, 3898.
[62] U. Aslam, V. G. Rao, S. Chavez, S. Linic, *Nat. Catal.* **2018**, *1*, 656–665.
[63] L. Buglioni, F. Raymenants, A. Slattery, S. D. A. Zondag, T. Noël, *Chem. Rev.* **2022**, *122*, 2752–2906.
[64] G. Ozin, *Matter* **2022**, *5*, 2594–2614.
[65] G. Baffou, I. Bordacchini, A. Baldi, R. Quidant, *Light Sci. Appl.* **2020**, *9*, 1–16.
[66] X. Zhang, X. Li, M. E. Reish, D. Zhang, N. Q. Su, Y. Gutiérrez, F. Moreno, W. Yang, H. O. Everitt, J. Liu, *Nano Lett.* **2018**, *18*, 1714–1723.
[67] R. Grote, R. Habets, J. Rohlfs, F. Sastre, N. Meulendijks, M. Xu, M. A. Verheijen, K. Elen, A. Hardy, M. K. Van Bael, T. Hartog, P. Buskens, *ChemCatChem* **2020**, *12*, 5618–5622.
[68] I. W. Un, Y. Sivan, *Nanoscale* **2020**, *12*, 17821–17832.
[69] J. Hong, C. Xu, B. Deng, Y. Gao, X. Zhu, X. Zhang, Y. Zhang, *Adv. Sci.* **2022**, *9*, 2103926.
[70] M.-J. Cai, C.-R. Li, L. He, *Rare Met.* **2020**, *39*, 881–886.
[71] I. W. Un, Y. Dubi, Y. Sivan, *Nanoscale* **2022**, *14*, 5022–5032.
[72] M. Xu, T. den Hartog, L. Cheng, M. Wolfs, R. Habets, J. Rohlfs, J. van den Ham, N. Meulendijks, F. Sastre, P. Buskens, *ChemPhotoChem* **2022**, *6*, e202100289.
[73] L. Mascaretti, A. Schirato, T. Montini, A. Alabastri, A. Naldoni, P. Fornasiero, *Joule* **2022**, *6*, 1727–1732.
[74] V. H. Nguyen, B. S. Nguyen, Z. Jin, M. Shokouhimehr, H. W. Jang, C. Hu, P. Singh, P. Raizada, W. Peng, S. Shiung Lam, C. Xia, C. C. Nguyen, S. Y. Kim, Q. Van Le, *Chem. Eng. J.* **2020**, *402*, 126184.
[75] K. Li, X. An, K. H. Park, M. Khraisheh, J. Tang, *Catal. Today* **2014**, *224*, 3–12.

© 2023 The Authors. ChemSusChem published by Wiley-VCH GmbH

1864564x, 2024, 4, Downloaded from https://chemistry-europe.onlinelibrary.wiley.com/doi/10.1002/cssc.202301405 by Uva Universiteitsbibliotheek, Wiley Online Library on [02/05/2024]. See the Terms and Conditions (https://onlinelibrary.wiley.com/terms-and-conditions) on Wiley Online Library for rules of use; OA articles are governed by the applicable Creative Commons License

[76] Y. Izumi, *Coord. Chem. Rev.* **2013**, *257*, 171–186.
[77] Y. Wang, D. He, H. Chen, D. Wang, *J. Photochem. Photobiol. C* **2019**, *40*, 117–149.
[78] Y. Dong, P. Duchesne, A. Mohan, K. K. Ghuman, P. Kant, L. Hurtado, U. Ulmer, J. Y. Y. Loh, A. A. Tountas, L. Wang, A. Jelle, M. Xia, R. Dittmeyer, G. A. Ozin, *Chem. Soc. Rev.* **2020**, *49*, 5648–5663.
[79] Z. Chen, W. Wei, B. J. Ni, *Curr. Opin. Green Sustain. Chem.* **2021**, *27*, 100398.
[80] P. Subramanyam, B. Meena, V. Biju, H. Misawa, S. Challapalli, *J. Photochem. Photobiol. C* **2022**, *51*, 100472.
[81] L. J. Minggu, W. R. Wan Daud, M. B. Kassim, *Int. J. Hydrogen Energy* **2010**, *35*, 5233–5244.
[82] S. Li, S. Haussener, *Appl. Energy* **2023**, *334*, 120617.
[83] F. M. Akwi, P. Watts, *Chem. Commun.* **2018**, *54*, 13894–13928.
[84] C. Holtze, R. Boehling, *Curr. Opin. Chem. Eng.* **2022**, *36*, 100798.
[85] D. Dallinger, B. Gutmann, C. O. Kappe, *Acc. Chem. Res.* **2020**, *53*, 1330–1341.
[86] S. Ali, M. C. Flores, A. Razzaq, S. Sorcar, C. B. Hiragond, H. R. Kim, Y. H. Park, Y. Hwang, H. S. Kim, H. Kim, E. H. Gong, J. Lee, D. Kim, S.-I. In, *Catalysts* **2019**, *9*, 727.
[87] Y. Li, S. Zhang, Q. Yu, W. Yin, *Appl. Surf. Sci.* **2007**, *253*, 9254–9258.
[88] R. J. White, R. Luque, V. L. Budarin, J. H. Clark, D. J. Macquarrie, *Chem. Soc. Rev.* **2009**, *38*, 481–494.
[89] A. Pistone, D. Iannazzo, M. Fazio, F. Celegato, G. Barrera, P. Tiberto, A. Giordano, B. Azzerboni, S. Galvagno, *Phys. Condens. Matter* **2014**, *435*, 88–91.
[90] R. Zanella, S. Giorgio, C. R. Henry, C. Louis, *J. Phys. Chem. B* **2002**, *106*, 7634–7642.
[91] C. Dette, M. A. Pérez-Osorio, C. S. Kley, P. Punke, C. E. Patrick, P. Jacobson, F. Giustino, S. J. Jung, K. Kern, *Nano Lett.* **2014**, *14*, 6533–6538.
[92] V. Etacheri, C. Di Valentin, J. Schneider, D. Bahnemann, S. C. Pillai, *J. Photochem. Photobiol. C* **2015**, *25*, 1–29.
[93] P. S. Basavarajappa, S. B. Patil, N. Ganganagappa, K. R. Reddy, A. V. Raghu, C. V. Reddy, *Int. J. Hydrogen Energy* **2020**, *45*, 7764–7778.
[94] G. A. Ozin, *Adv. Mater.* **2015**, *27*, 1957–1963.
[95] C. McCullagh, N. Skillen, M. Adams, P. K. J. Robertson, *J. Chem. Technol. Biotechnol.* **2011**, *86*, 1002–1017.
[96] L. Liu, H. Zhao, J. M. Andino, Y. Li, *ACS Catal.* **2012**, *2*, 1817–1828.
[97] Q. Zhang, Y. Li, E. A. Ackerman, M. Gajdardziska-Josifovska, H. Li, *Appl. Catal. A* **2011**, *400*, 195–202.
[98] H. Zhao, L. Liu, J. M. Andino, Y. Li, *J. Mater. Chem. A* **2013**, *1*, 8209–8216.
[99] L. Liu, Y. Jiang, H. Zhao, J. Chen, J. Cheng, K. Yang, Y. Li, *ACS Catal.* **2016**, *6*, 1097–1108.
[100] S. Sorcar, Y. Hwang, C. A. Grimes, S. Il In, *Mater. Today* **2017**, *20*, 507–515.
[101] H. Bian, T. Liu, D. Li, Z. Xu, J. Lian, M. Chen, J. Yan, S. Frank Liu, *Chem. Eng. J.* **2022**, *435*, 135071.
[102] Y. Wang, X. Wang, M. Antonietti, *Angew. Chem. Int. Ed.* **2012**, *51*, 68–89.
[103] J. Fu, J. Yu, C. Jiang, B. Cheng, *Adv. Energy Mater.* **2018**, *8*, 1701503.
[104] S. Mazzanti, A. Savateev, *ChemPlusChem* **2020**, *85*, 2499–2517.
[105] W.-J. Ong, L.-L. Tan, Y. H. Ng, S.-T. Yong, S.-P. Chai, *Chem. Rev.* **2016**, *116*, 7159–7329.
[106] X. Wang, K. Maeda, A. Thomas, K. Takanabe, G. Xin, J. M. Carlsson, K. Domen, M. Antonietti, *Nat. Mater.* **2009**, *8*, 76–80.
[107] L. B. Hoch, T. E. Wood, P. G. O'Brien, K. Liao, L. M. Reyes, C. A. Mims, G. A. Ozin, *Adv. Sci.* **2014**, *1*, 1400013.
[108] K. K. Ghuman, T. E. Wood, L. B. Hoch, C. A. Mims, G. A. Ozin, C. V. Singh, *Phys. Chem. Chem. Phys.* **2015**, *17*, 14623–14635.
[109] T. Yan, L. Wang, Y. Liang, M. Makaremi, T. E. Wood, Y. Dai, B. Huang, A. A. Jelle, Y. Dong, G. A. Ozin, *Nat. Commun.* **2019**, *10*, 2521.
[110] Y. Dong, K. Kaur Ghuman, R. Popescu, P. N. Duchesne, W. Zhou, J. Y. Y. Loh, A. A. Jelle, J. Jia, D. Wang, X. Mu, C. Kübel, L. Wang, L. He, M. Ghoussoub, Q. Wang, T. E. Wood, L. M. Reyes, P. Zhang, N. P. Kherani, C. Veer Singh, G. A. Ozin, *Adv. Sci.* **2018**, *5*, 1700732.
[111] L. Wang, Y. Dong, T. Yan, Z. Hu, A. A. Jelle, D. M. Meira, P. N. Duchesne, J. Y. Y. Loh, C. Qiu, E. E. Storey, Y. Xu, W. Sun, M. Ghoussoub, N. P. Kherani, A. S. Helmy, G. A. Ozin, *Nat. Commun.* **2020**, *11*, 2432.
[112] A. Sial, A. A. Dar, Y. Li, C. Wang, *Photochemistry* **2022**, *2*, 810–830.
[113] P. Cheng, D. Wang, P. Schaaf, *Adv. Sustainable Syst.* **2022**, *6*, 2200115.
[114] B. Xie, E. Lovell, T. H. Tan, S. Jantarang, M. Yu, J. Scott, R. Amal, *J. Energy Chem.* **2021**, *59*, 108–125.
[115] C. Clavero, *Nat. Photonics* **2014**, *8*, 95–103.
[116] D. Mateo, P. Maity, G. Shterk, O. F. Mohammed, J. Gascon, *ChemSusChem* **2021**, *14*, 5525–5533.
[117] Y. Li, Z. Zeng, Y. Zhang, Y. Chen, W. Wang, X. Xu, M. Du, Z. Li, Z. Zou, *ACS Sustainable Chem. Eng.* **2022**, *10*, 6382–6388.
[118] P. K. Jain, X. Huang, I. H. El-Sayed, M. A. El-Sayed, *Acc. Chem. Res.* **2008**, *41*, 1578–1586.
[119] S. Sorcar, Y. Hwang, J. Lee, H. Kim, K. M. Grimes, C. A. Grimes, J.-W. W. Jung, C.-H. H. Cho, T. Majima, M. R. Hoffmann, S.-I. Il In, *Energy Environ. Sci.* **2019**, *12*, 2685–2696.
[120] S. Ali, J. Lee, H. Kim, Y. Hwang, A. Razzaq, J.-W. Jung, C.-H. Cho, S.-I. In, *Appl. Catal. B* **2020**, *279*, 119344.
[121] L. Wan, Q. Zhou, X. Wang, T. E. Wood, L. Wang, P. N. Duchesne, J. Guo, X. Yan, M. Xia, Y. F. Li, A. A. Jelle, U. Ulmer, J. Jia, T. Li, W. Sun, G. A. Ozin, *Nat. Catal.* **2019**, *2*, 889–898.
[122] J. Guo, P. N. Duchesne, L. Wang, R. Song, M. Xia, U. Ulmer, W. Sun, Y. Dong, J. Y. Y. Loh, N. P. Kherani, J. Du, B. Zhu, W. Huang, S. Zhang, G. A. Ozin, *ACS Catal.* **2020**, *10*, 13668–13681.
[123] P. M. Molina, K. W. Bossers, J. D. Wienk, J. Rohlfs, N. Meulendijks, M. A. Verheijen, P. Buskens, F. Sastre, *Chem. Asian J.* **2023**, *18(14)*, e202300405, DOI 10.1002/asia.202300405.
[124] A. A. Upadhye, I. Ro, X. Zeng, H. J. Kim, I. Tejedor, M. A. Anderson, J. A. Dumesic, G. W. Huber, *Catal. Sci. Technol.* **2015**, *5*, 2590–2601.
[125] P. Martínez Molina, N. Meulendijks, M. Xu, M. A. Verheijen, T. Hartog, P. Buskens, F. Sastre, *ChemCatChem* **2021**, *13*, 4507–4513.
[126] J. Volders, K. Elen, A. Raes, R. Ninakanti, A.-S. Kelchtermans, F. Sastre, A. Hardy, P. Cool, S. W. Verbruggen, P. Buskens, M. K. Van Bael, *Nanomaterials* **2022**, *12*, 4153.
[127] A. O. Govorov, H. H. Richardson, *Nano Today* **2007**, *2*, 30–38.
[128] H. Li, Y. Gao, Z. Xiong, C. Liao, K. Shih, *Appl. Surf. Sci.* **2018**, *439*, 552–559.
[129] M. Tahir, B. Tahir, M. G. M. Nawawi, M. Hussain, A. Muhammad, *Appl. Surf. Sci.* **2019**, *485*, 450–461.
[130] Y. F. Li, N. Soheilnia, M. Greiner, U. Ulmer, T. Wood, F. M. Ali, Y. Dong, A. P. Yin Wong, J. Jia, G. A. Ozin, *ACS Appl. Mater. Interfaces* **2019**, *11*, 5610–5615.
[131] H. Ge, Y. Kuwahara, K. Kusu, H. Kobayashi, H. Yamashita, *J. Mater. Chem. A* **2022**, *10*, 10854–10864.
[132] Y. F. Li, W. Lu, K. Chen, P. Duchesne, F. M. Ali, M. Xia, T. E. Wood, U. Ulmer, G. A. Ozin, *J. Am. Chem. Soc.* **2019**, *141*, 14991–14996.
[133] J. M. Sanz, D. Ortiz, R. Alcaraz de la Osa, J. M. Saiz, F. González, A. S. Brown, M. Losurdo, H. O. Everitt, F. Moreno, *J. Phys. Chem. C* **2013**, *117*, 19606–19615.
[134] L. Cui, S. Mahajan, R. M. Cole, B. Soares, P. N. Bartlett, J. J. Baumberg, I. P. Hayward, B. Ren, A. E. Russell, Z. Q. Tian, *Phys. Chem. Chem. Phys.* **2009**, *11*, 1023–1026.
[135] Y. Tang, S. Wu, Y. Wang, L. Song, Z. Yang, C. Guo, J. Liu, F. Wang, *Energy Fuels* **2023**, *37*, 539–546.
[136] J. Rohlfs, K. W. Bossers, N. Meulendijks, F. Valega Mackenzie, M. Xu, M. A. Verheijen, P. Buskens, F. Sastre, *Catalysts* **2022**, *12*, 126.
[137] D. Mateo, J. Albero, H. García, *Joule* **2019**, *3*, 1949–1962.
[138] Z. Wu, C. Li, Z. Li, K. Feng, M. Cai, D. Zhang, S. Wang, M. Chu, C. Zhang, J. Shen, Z. Huang, Y. Xiao, G. A. Ozin, X. Zhang, L. He, *ACS Nano* **2021**, *15*, 5696–5705.
[139] F. Sastre, C. Versluis, N. Meulendijks, J. Rodríguez-Fernández, J. Sweelssen, K. Elen, M. K. Van Bael, T. den Hartog, M. A. Verheijen, P. Buskens, *ACS Omega* **2019**, *4*, 7369–7377.
[140] F. Sastre, A. V. Puga, L. Liu, A. Corma, H. García, *J. Am. Chem. Soc.* **2014**, *136*, 6798–6801.
[141] X. Meng, T. Wang, L. Liu, S. Ouyang, P. Li, H. Hu, T. Kako, H. Iwai, A. Tanaka, J. Ye, *Angew. Chem. Int. Ed.* **2014**, *53*, 11478–11482.
[142] D. Burova, J. Rohlfs, F. Sastre, P. M. Molina, N. Meulendijks, M. A. Verheijen, A.-S. Kelchtermans, K. Elen, A. Hardy, M. K. Van Bael, P. Buskens, *Catalysts* **2022**, *12*, 284.
[143] K. Jalama, *Catal. Rev. Sci. Eng.* **2017**, *59*, 95–164.
[144] Z. Li, R. Shi, J. Zhao, T. Zhang, *Nano Res.* **2021**, *14*, 4828–4832.
[145] J. Ren, S. Ouyang, H. Xu, X. Meng, T. Wang, D. Wang, J. Ye, *Adv. Energy Mater.* **2017**, *7*, 1601657.
[146] S. Jantarang, S. Ligori, J. Horlyck, E. Lovell, T. Tan, B. Xie, R. Amal, J. Scott, *Materials (Basel).* **2021**, *14*, 4195.
[147] S. Ullah, E. C. Lovell, R. J. Wong, T. H. Tan, J. Scott, R. Amal, *ACS Sustainable Chem. Eng.* **2020**, *8*, 5056–5066.
[148] S. Ullah, E. C. Lovell, T. H. Tan, B. Xie, P. V. Kumar, R. Amal, J. Scott, *Appl. Catal. B* **2021**, *294*, 120248.
[149] K. Peng, J. Ye, H. Wang, H. Song, B. Deng, S. Song, Y. Wang, L. Zuo, J. Ye, *Appl. Catal. B* **2023**, *324*, 122262.

© 2023 The Authors. ChemSusChem published by Wiley-VCH GmbH

1864564x, 2024, 4, Downloaded from https://chemistry-europe.onlinelibrary.wiley.com/doi/10.1002/cssc.202301405 by Uva Universiteitsbibliotheek, Wiley Online Library on [02/05/2024]. See the Terms and Conditions (https://onlinelibrary.wiley.com/terms-and-conditions) on Wiley Online Library for rules of use; OA articles are governed by the applicable Creative Commons License

[150] I. Ro, C. Sener, T. M. Stadelman, M. R. Ball, J. M. Venegas, S. P. Burt, I. Hermans, J. A. Dumesic, G. W. Huber, *J. Catal.* **2016**, *344*, 784–794.
[151] Y.-F. Xu, P. N. Duchesne, L. Wang, A. Tavasoli, F. M. Ali, M. Xia, J.-F. Liao, D.-B. Kuang, G. A. Ozin, *Nat. Commun.* **2020**, *11*, 5149.
[152] J. Jia, H. Wang, Z. Lu, P. G. O'Brien, M. Ghoussoub, P. Duchesne, Z. Zheng, P. Li, Q. Qiao, L. Wang, A. Gu, F. M. Ali, Y. Dong, Q. Wang, K. K. Ghuman, T. Wood, C. Qian, Y. Shao, C. Qiu, M. Ye, Y. Zhu, Z. Lu, P. Zhang, A. S. Helmy, C. V. Singh, N. P. Kherani, D. D. Perovic, G. A. Ozin, *Adv. Sci.* **2017**, *4*, 1700252.
[153] H. Zhang, T. Wang, J. Wang, H. Liu, T. D. Dao, M. Li, G. Liu, X. Meng, K. Chang, L. Shi, T. Nagao, J. Ye, *Adv. Mater.* **2016**, *28*, 3703–3710.
[154] Y. Tang, Z. Yang, C. Guo, H. Han, Y. Jiang, Z. Wang, J. Liu, L. Wu, F. Wang, *J. Mater. Chem. A* **2022**, *10*, 12157–12167.
[155] P. K. Jain, M. A. El-Sayed, *Chem. Phys. Lett.* **2010**, *487*, 153–164.
[156] D. Liu, C. Xue, *Adv. Mater.* **2021**, *33*, 2005738.
[157] A. Chaudhuri, S. D. A. Zondag, J. H. A. Schuurmans, J. van der Schaaf, T. Noël, *Org. Process Res. Dev.* **2022**, *26*, 1279–1288.
[158] D. Cambié, C. Bottecchia, N. J. W. Straathof, V. Hessel, T. Noël, *Chem. Rev.* **2016**, *116*, 10276–10341.
[159] X. T. Cao, D. M. Kabtamu, S. Kumar, R. S. Varma, *ACS Sustainable Chem. Eng.* **2022**, *10*, 12906–12932.
[160] S. D. A. Zondag, T. M. Masson, M. G. Debije, T. Noël, *Photochem. Photobiol. Sci.* **2022**, *21*, 705–717.
[161] D. Cambié, T. Noël, *Top. Curr. Chem.* **2018**, *376*, 45.
[162] H. P. L. Gemoets, Y. Su, M. Shang, V. Hessel, R. Luque, T. Noël, *Chem. Soc. Rev.* **2016**, *45*, 83–117.
[163] N. Kockmann, P. Thenée, C. Fleischer-Trebes, G. Laudadio, T. Noël, *React. Chem. Eng.* **2017**, *2*, 258–280.
[164] M. Movsisyan, E. I. P. Delbeke, J. K. E. T. Berton, C. Battilocchio, S. V. Ley, C. V. Stevens, *Chem. Soc. Rev.* **2016**, *45*, 4892–4928.
[165] Z. Dong, Z. Wen, F. Zhao, S. Kuhn, T. Noël, *Chem. Eng. Sci.* **2021**, *10*, 100097.
[166] Z. Dong, S. D. A. Zondag, M. Schmid, Z. Wen, T. Noël, *Chem. Eng. J.* **2022**, *428*, 130968.
[167] H. Kisch, *Angew. Chem.* **2010**, *122*, 9782–9783.
[168] Z. Wang, T. Hisatomi, R. Li, K. Sayama, G. Liu, K. Domen, C. Li, L. Wang, *Joule* **2021**, *5*, 344–359.
[169] X. Li, X. Zhang, H. O. Everitt, J. Liu, *Nano Lett.* **2019**, *19*, 1706–1711.
[170] N. Keller, J. Ivanez, J. Highfield, A. M. Ruppert, *Appl. Catal. B* **2021**, *296*, 120320.
[171] I.-W. Un, Y. Sivan, *ACS Photonics* **2021**, *8*, 1183–1190.
[172] Y. Dubi, I. W. Un, Y. Sivan, *Chem. Sci.* **2020**, *11*, 5017–5027.
[173] V. Vaiano, D. Sannino, P. Ciambelli, *Chem. Eng. Trans.* **2015**, *43*, 1003–1008.
[174] Z. Y. Wang, H. C. Chou, J. C. S. Wu, D. Ping Tsai, G. Mul, C. Engineering, *Appl. Catal. A* **2010**, *380*, 172–177.
[175] A. Mohan, U. Ulmer, L. Hurtado, J. Loh, Y. F. Li, A. A. Tountas, C. Krevert, C. Chan, Y. Liang, P. Brodersen, M. M. Sain, G. A. Ozin, *ACS Appl. Mater. Interfaces* **2020**, *12*, 33613–33620.
[176] T. Wang, L. Yang, K. Yuan, X. Du, Y. Yang, *Energy Convers. Manage.* **2014**, *87*, 606–617.
[177] V. Esen, Ş. Sağlam, B. Oral, *Renewable Sustainable Energy Rev.* **2017**, *77*, 1240–1250.
[178] T. Claes, A. Dilissen, M. E. Leblebici, T. Van Gerven, *Chem. Eng. J.* **2019**, *361*, 725–735.
[179] S. D. A. Zondag, D. Mazzarella, T. Noël, *Annu. Rev. Chem. Biomol. Eng.* **2023**, *14*, 283–300.
[180] D. J. Walsh, T. N. Schneider, B. D. Olsen, K. F. Jensen, *React. Chem. Eng.* **2023**, *8*, 416–423.
[181] M. Sender, D. Ziegenbalg, *React. Chem. Eng.* **2021**, *6*, 1614–1627.
[182] T. M. Masson, S. D. A. Zondag, K. P. L. Kuijpers, D. Cambié, M. G. Debije, T. Noël, *ChemSusChem* **2021**, *14*, 5417–5423.
[183] A. Gallo, A. Marzo, E. Fuentealba, E. Alonso, *Renewable Sustainable Energy Rev.* **2017**, *77*, 1385–1402.
[184] M. Tanveer, G. Tezcanli Guyer, *Renewable Sustainable Energy Rev.* **2013**, *24*, 534–543.
[185] E. T. Kho, T. H. Tan, E. Lovell, R. J. Wong, J. Scott, R. Amal, *Green Energy & Environ.* **2017**, *2*, 204–217.
[186] A. Vidal, *Chemosphere* **1998**, *36*, 2593–2606.
[187] P. P. Dutta, S. S. Begum, H. Jangid, A. P. Goswami, T. Doley, M. Bardalai, P. P. Dutta, *Mater. Today: Proc.* **2021**, *47*, 4226–4234.
[188] Z. Zhang, Y. Wang, G. Cui, H. Lu, S. Abanades, *Appl. Phys. Lett.* **2021**, *119*, 123906.
[189] L. Xu, Y. Ren, Y. Fu, M. Liu, F. Zhu, M. Cheng, J. Zhou, W. Chen, K. Wang, N. Wang, N. Li, *Chem. Eng. J.* **2023**, *468*, 143831.
[190] P. Furler, J. Scheffe, M. Gorbar, L. Moes, U. Vogt, A. Steinfeld, *Energy Fuels* **2012**, *26*, 7051–7059.
[191] W. C. Chueh, C. Falter, M. Abbott, D. Scipio, P. Furler, S. M. Haile, A. Steinfeld, *Science.* **2010**, *330*, 1797–1801.
[192] A. Le Gal, S. Abanades, G. Flamant, *Energy Fuels* **2011**, *25*, 4836–4845.
[193] C. Agrafiotis, H. von Storch, M. Roeb, C. Sattler, *Renewable Sustainable Energy Rev.* **2014**, *29*, 656–682.
[194] D. Bahnemann, *Sol. Energy* **2004**, *77*, 445–459.
[195] A. Vilanova, P. Dias, J. Azevedo, M. Wullenkord, C. Spenke, T. Lopes, A. Mendes, *J. Power Sources* **2020**, *454*, 227890.
[196] M. M. Kandy, V. G. Gaikar, *Renewable Energy* **2019**, *139*, 915–923.
[197] H. Wang, S. Fu, B. Shang, S. Jeon, Y. Zhong, N. J. Harmon, C. Choi, E. A. Stach, H. Wang, *Angew. Chem.* **2023**, *135*, e202305251, DOI 10.1002/ange.202305251.
[198] X. Chen, Q. Li, M. Zhang, J. Li, S. Cai, J. Chen, H. Jia, *ACS Appl. Mater. Interfaces* **2020**, *12*, 39304–39317.
[199] X. Fang, Z. Gao, H. Lu, Z. Zhang, *Catal. Commun.* **2019**, *125*, 48–51.
[200] Z. Zhang, Z. Gao, H. Liu, S. Abanades, H. Lu, *ACS Appl. Energ. Mater.* **2019**, *2*, 8376–8380.
[201] Y. Liu, F. Yu, F. Wang, S. Bai, G. He, *Jiegou Huaxue* **2022**, *41*, 2201034–2201039.
[202] V. Sumathi, R. Jayapragash, A. Bakshi, P. Kumar Akella, *Renewable Sustainable Energy Rev.* **2017**, *74*, 130–138.
[203] A. X. Maldonado Pérez, J. de J. Pérez Bueno, *Rev. Adv. Mater. Sci.* **2023**, *62*, 20220293, DOI 10.1515/rams-2022-0293.
[204] H. Zhang, H. Chen, Y. Han, H. Liu, M. Li, *Renewable Energy* **2017**, *113*, 784–794.
[205] F. Cao, L. Wang, T. Zhu, *Int. J. Photoenergy* **2017**, *2017*, 1–7.
[206] M. Wullenkord, C. Jung, C. Sattler, in *Vol. 1 Comb. Energy Cycles, CHP, CCHP, Smart Grids; Conc. Sol. Power, Sol. Thermochem. Therm. Energy Storage; Geothermal, Ocean. Emerg. Energy Technol. Hydrog. Energy Technol. Low/Zero Emiss. Power Plants An*, American Society Of Mechanical Engineers, **2014**.
[207] B. M. da Costa Filho, A. L. P. Araujo, G. V. Silva, R. A. R. Boaventura, M. M. Dias, J. C. B. Lopes, V. J. P. Vilar, *Chem. Eng. J.* **2017**, *310*, 331–341.
[208] K. Tong, L. Yang, X. Du, Y. Yang, *Renewable Sustainable Energy Rev.* **2020**, *131*, 109986.
[209] X. Meng, Z. Zhang, *AIChE J.* **2019**, *65*, 132–139.
[210] J. Wang, Y. Xuan, J. Zeng, Q. Zhu, Z. Zhu, *Energy Convers. Manage.* **2023**, *281*, 116859.
[211] W. K. Fan, M. Tahir, *Chem. Eng. J.* **2022**, *427*, 131617.
[212] "Raman High Temperature Reaction Chamber – HVC-MRA-5 – Harrick Scientific Products Inc.," can be found under https://harricksci.com/raman-high-temperature-reaction-chamber-HVC-MRA-5/#product-tab-sa, **n.d**.
[213] J. Albero, E. Dominguez, A. Corma, H. García, *Sustain. Energy Fuels* **2017**, *1*, 1303–1307.
[214] C. J. Bueno-Alejo, A. Arca-Ramos, J. L. Hueso, J. Santamaria, *Catal. Today* **2020**, *355*, 678–684.
[215] M. Vezzoli, T. Farrell, A. Baker, S. Psaltis, W. N. Martens, J. M. Bell, *Chem. Eng. J.* **2013**, *234*, 57–65.
[216] G. Camera-Roda, F. Santarelli, *Catal. Today* **2007**, *129*, 161–168.
[217] T. Claes, T. Van Gerven, M. E. Leblebici, *Chem. Eng. J.* **2021**, *403*, 126355.
[218] A. Yusuf, C. Garlisi, G. Palmisano, *Catal. Today* **2018**, *315*, 79–92.
[219] P. S. Walko, R. N. Devi, *Int. J. Hydrogen Energy* **2023**, *48(45)*, 17086–17096, DOI 10.1016/J.IJHYDENE.2023.01.148.
[220] J. C. S. Wu, H.-M. Lin, C.-L. Lai, *Appl. Catal. A* **2005**, *296*, 194–200.
[221] T.-V. Nguyen, J. C. S. Wu, *Appl. Catal. A* **2008**, *335*, 112–120.
[222] T.-V. Nguyen, J. C. S. Wu, *Sol. Energy Mater. Sol. Cells* **2008**, *92*, 864–872.
[223] T.-V. Nguyen, J. C. S. Wu, C.-H. Chiou, *Catal. Commun.* **2008**, *9*, 2073–2076.
[224] P.-Y. Liou, S.-C. Chen, J. C. S. Wu, D. Liu, S. Mackintosh, M. Maroto-Valer, R. Linforth, *Energy Environ. Sci.* **2011**, *4*, 1487.
[225] S. Bhatta, D. Nagassou, S. Mohsenian, J. P. Trelles, *Sol. Energy* **2019**, *178*, 201–214.
[226] R. Munirathinam, J. Huskens, W. Verboom, *Adv. Synth. Catal.* **2015**, *357*, 1093–1123.
[227] A. Kirschning, W. Solodenko, K. Mennecke, *Chem. A Eur. J.* **2006**, *12*, 5972–5990.
[228] O. Ola, M. M. Maroto-Valer, *Chem. Eng. J.* **2016**, *283*, 1244–1253.
[229] J. Y. Y. Loh, A. Mohan, A. G. Flood, G. A. Ozin, N. P. Kherani, *Nat. Commun.* **2021**, *12*, 402.
[230] Y. Li, J. Hao, H. Song, F. Zhang, X. Bai, X. Meng, H. Zhang, S. Wang, Y. Hu, J. Ye, *Nat. Commun.* **2019**, *10*, 2359.

© 2023 The Authors. ChemSusChem published by Wiley-VCH GmbH

1864564x, 2024, 4, Downloaded from https://chemistry-europe.onlinelibrary.wiley.com/doi/10.1002/cssc.202301405 by Uva Universiteitsbibliotheek, Wiley Online Library on [02/05/2024]. See the Terms and Conditions (https://onlinelibrary.wiley.com/terms-and-conditions) on Wiley Online Library for rules of use; OA articles are governed by the applicable Creative Commons License

[231] L. Hurtado, A. Mohan, U. Ulmer, R. Natividad, A. A. Tountas, W. Sun, L. Wang, B. Kim, M. M. Sain, G. A. Ozin, *Chem. Eng. J.* **2022**, *435*, 134864.
[232] M. Cheng, S. Yang, R. Chen, X. Zhu, Q. Liao, Y. Huang, *J. Mol. Catal.* **2018**, *448*, 185–194.
[233] I. Ro, R. Carrasquillo-Flores, J. A. Dumesic, G. W. Huber, *Appl. Catal. A* **2016**, *521*, 182–189.
[234] B. Deng, H. Song, K. Peng, Q. Li, J. Ye, *Appl. Catal. B* **2021**, *298*, 120519.
[235] M. Cabrero-Antonino, B. Ferrer, H. G. Baldoví, S. Navalón, *Chem. Eng. J.* **2022**, *445*, 136426.

Manuscript received: September 29, 2023
Revised manuscript received: November 29, 2023
Accepted manuscript online: November 30, 2023
Version of record online: December 20, 2023

© 2023 The Authors. ChemSusChem published by Wiley-VCH GmbH

1864564x, 2024, 4, Downloaded from https://chemistry-europe.onlinelibrary.wiley.com/doi/10.1002/cssc.202301405 by Uva Universiteitsbibliotheek, Wiley Online Library on [02/05/2024]. See the Terms and Conditions (https://onlinelibrary.wiley.com/terms-and-conditions) on Wiley Online Library for rules of use; OA articles are governed by the applicable Creative Commons License